Geochemical Perspectives Letters

Wehrlites from continental mantle monitor the passage and degassing of carbonated melts

S. Aulbach[1*], A.-B. Lin[2,3], Y. Weiss[4], G.M. Yaxley[5]

OPEN ACCESS
doi: 10.7185/geochemlet.2031

Abstract

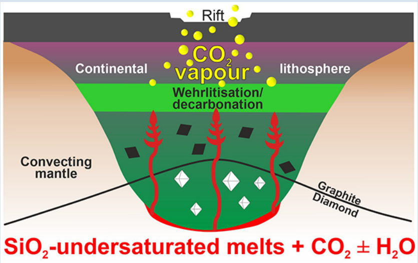

Continental rifting has been linked to the thinning and destruction of cratonic lithosphere and to the release of enough CO_2 to impact the global climate. This fundamental plate tectonic process facilitates the infiltration and mobilisation of small-volume carbonated melts, which may interact with mantle peridotite to form wehrlite through the reaction: enstatite + dolomite (melt) = forsterite + diopside + CO_2 (vapour). Application to mantle xenolith suites from various rifts and basins shows that 2.9 to 10.2 kg CO_2 are released *per* 100 kg of wehrlite formed. For the Eastern Rift (Africa), this results in estimated CO_2 fluxes of 6.5 ± 4.1 Mt yr^{-1}, similar to estimates of mantle contributions based on surficial CO_2 surveys. Thus, wehrlite-bearing xenolith suites can be used to monitor present and past CO_2 mobility through the continental lithosphere, ultimately with diffuse degassing to the atmosphere. They may also reveal the CO_2 flux in lithospheric provinces where carbonated melts or continent-scale rifts are not observed at the surface.

Received 2 May 2020 | Accepted 17 August 2020 | Published 25 September 2020

Introduction

The conversion of lherzolite and harzburgite to an orthopyroxene-poor or -free, clinopyroxene-rich rock classified as wehrlite – a process hereafter referred to as wehrlitisation – requires interaction with silica-undersaturated (ultra)basic melts (*e.g.*, Wallace and Green, 1988; Yaxley *et al.*, 1998). Such melts encompass carbonatites, carbonated silicate melts (*e.g.*, kimberlite) or CO_2-bearing silicate melts (*e.g.*, melilitites and nephelinites), which can form by near-solidus melting of peridotite (*e.g.*, Gudfinnsson and Presnall, 2005). Given the strong incompatibility of CO_2 in peridotite, low-volume melts are typically carbonated even if the source is not specifically C-rich, as long as the mantle source lies above the depth of redox melting (Hirschmann, 2010). In extensional continental settings, small-volume melts generated in the deep lithospheric or convecting mantle traverse ~100 to 250 km of subcontinental lithospheric mantle (SCLM) and crust, with which they are initially out of chemical equilibrium, causing extensive reactions to occur (*e.g.*, McKenzie, 1989). Wehrlitisation can result from such reactions and involves the liberation of CO_2 vapour (*e.g.*, Wallace and Green, 1988; Yaxley *et al.*, 1998). This, in turn, contributes to diffuse continental degassing, especially in rift settings where lithosphere thinning has occurred (Brune *et al.*, 2017; Foley and Fischer, 2017). It is noticeable that wehrlites are frequently reported in the literature for basalt-borne xenolith suites associated with rifts, faults and basins. These structures are pathways for CO_2-rich fluids (Tamburello *et al.*, 2018). However, a link between the release of CO_2 to the exosphere during diffuse, non-volcanic degassing and a specific petrological mechanism remains unexplored, and the passage of carbon through the lithosphere is itself poorly documented. Wehrlite-bearing xenolith suites have been entrained in magmas of various ages. Using literature data, we show that wehrlites, as both products and monitors of the passage of CO_2-bearing melts, can reveal the otherwise hidden CO_2 flux through the shallow SCLM, and its eventual tectonic degassing both in currently and formerly active rifts.

Depths, Hallmarks and Agents of Wehrlitisation

Published data show that basalt-borne xenolith suites from the spinel facies SCLM (~40–100 km), mostly associated with off-cratonic lithosphere or cratonic lithosphere in various states of disruption and decratonisation, contain significant proportions of wehrlite (Table S-1). The data compilation encompasses garnet-free xenoliths from various on- and off-cratonic rift systems and basins (Supplementary Information). Indeed, the decarbonation reaction, which causes wehrlitisation, has been experimentally demonstrated to occur at relatively shallow depths corresponding to ~1.5 to 2.0 GPa (Wallace and Green, 1988, and references therein). This is because the carbonated peridotite solidus features a "ledge" in pressure-temperature space so that on upward movement of carbonatite melts, they must freeze and react to form wehrlites (Wallace and Green

1. Institute of Geosciences, Goethe-Universität, 60438 Frankfurt am Main, Germany
2. School of Earth Sciences, State Key Laboratory of Geological Processes and Mineral Resources, China University of Geosciences, Wuhan 430074, China
3. State Key Laboratory of Continental Dynamics, Department of Geology, Northwest University, Xi'an 710069, China
4. The Freddy and Nadine Herrmann Institute of Earth Sciences, The Hebrew University, 91904 Jerusalem, Israel
5. Research School of Earth Sciences, The Australian National University, Canberra ACT 2601, Australia
* Corresponding author (email: s.aulbach@em.uni-frankfurt.de)

1988). There is pervasive evidence for the interaction of SiO_2-undersaturated, CO_2-bearing melts also with the deep lithosphere, and carbonatitic high-density fluids are observed in diamonds (Fig. 1, Table S-2). Nevertheless, the proportion of wehrlitic garnet both in xenoliths and as inclusions in diamond is minute (~1 %) compared to the lherzolite or harzburgite paragenesis (Fig. S-1). Thus, wehrlitisation is not an important process in the garnet- and diamond-stable part of the SCLM (>~60 and ~120 km, respectively, depending on geotherm), which typically records lower oxygen fugacities than the shallow SCLM (Supplementary Information). Interaction of carbonated melts with the deep lithosphere leads to graphite/diamond precipitation instead, through a process called redox freezing (Rohrbach and Schmidt, 2011).

Wehrlitisation leads to high clinopyroxene modes at the expense of orthopyroxene relative to other peridotites in the same xenolith suite. Transitional rock types affected by the same process, but at lower melt-rock ratios, also occur, resulting in

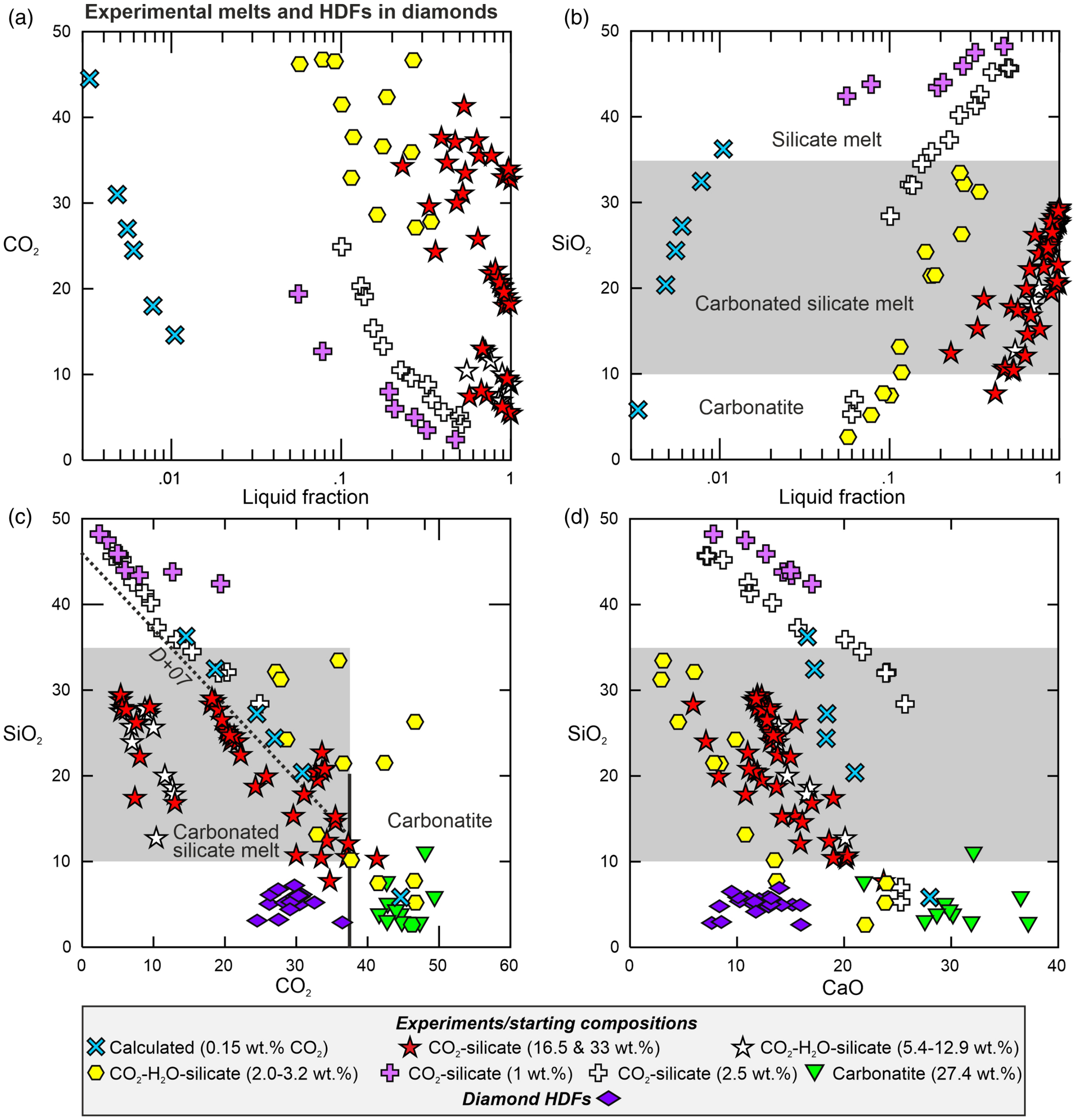

Figure 1 **(a-d)** Major element (wt. %) relationships and fractions of liquids ranging from carbonatite to carbonated silicate melt and silica-undersaturated, CO_2-($\pm H_2O$) bearing silicate melt produced in experiments; high-density fluids (HDFs) in diamonds (Table S-2) shown for comparison. Concentrations of CO_2 in the starting mixture are given in parentheses. Differences in liquid composition relate to different starting mixtures, but similarly sloping trends are obtained for the various studies. Trend and separation of carbonatite from carbonated silicate melt in **(c)** are from Dasgupta *et al.* (2007). Melt fractions are not reported in all experiments.

clinopyroxene-rich lherzolites and orthopyroxene-poor harzburgites with clinopyroxene/orthopyroxene ratios >1 (*e.g.*, Yaxley and Green, 1996; Lin *et al.*, 2020). Depending on the style of melt interaction (porous flow *vs.* fractures), olivine-rich, pyroxene-poor to -free dunites may ultimately form (*e.g.*, Shaw *et al.*, 2018). The metasomatic agents inferred for the various wehrlite-bearing xenolith suites range from carbonatite to carbonated silicate melts to CO_2-bearing silicate melts (Supplementary Information), which reflect increasing melt volumes and dilution with silicate components (*e.g.*, Gudfinnsson and Presnall, 2005). Based on experimentally produced melts, there is a relationship between melt fraction and CO_2 (Fig. 1a) and SiO_2 content (Fig. 1b), producing an inverse correlation between CO_2 and SiO_2 (Fig. 1c) and between SiO_2 and CaO (Fig. 1d). The higher melt volumes involved in the generation of SiO_2-rich melts may therefore compensate for their lower CO_2 contents in terms of their ability to convert a given amount of orthopyroxene to clinopyroxene. The link between silica-undersaturated carbonated melts, wehrlites and decarbonation at low pressure is strengthened by direct observations of CO_2-rich fluid inclusions, carbonates, carbonate-bearing glass veins and melt pockets in wehrlites, with entrapment pressures of 0.8 to 1.7 GPa (*e.g.*, Yaxley *et al.*, 1998; Loges *et al.*, 2019). It is further supported by experimental studies which show that wehrlite forms in equilibrium with carbonated melts (Yaxley and Green, 1996; Gervasoni *et al.*, 2017).

The effects of wehrlitisation on major element contents vary (Fig. S-2), reflecting the spectrum of SiO_2-undersaturated carbonated melts. In some suites (*e.g.*, Eifel, North Atlantic Craton in Greenland), clinopyroxene in wehrlite is dominated by elevated CaO/Al_2O_3 (Figs. 2a, S-2), in others by elevated FeO (Fig. 2b). The effects on the trace element budget are also heterogeneous (Fig. S-3), depending not only on the identity of the metasomatic agent and type of melt-rock reaction, but also on lithosphere thickness, as the melt traverses and equilibrates with garnet-bearing peridotite in thick lithospheres (Supplementary Information).

Modelling CO_2 Loss Via Wehrlitisation

The amount of CO_2 liberated from a volume of wehrlite-bearing peridotite due to interaction with CO_2-bearing, silica-undersaturated melt is estimated based on the decarbonation reaction

$$\underset{\text{Enstatite}}{4MgSiO_3} + \underset{\text{Dolomite}}{CaMg(CO_3)_2} = \underset{\text{Forsterite}}{2Mg_2SiO_4} + \underset{\text{Diopside}}{CaMgSi_2O_6} + \underset{\text{Vapour}}{2CO_2} \qquad \text{(Eq. 1)}$$

(*e.g.*, Yaxley and Green, 1996). Dolomite is assumed to be dissolved in the metasomatic melt, and wehrlites with high clinopyroxene modes formed from lherzolites and harzburgites with lower clinopyroxene modes (Wallace and Green, 1988; Yaxley *et al.*, 1998). The proportion of a rock mass affected by wehrlitisation is estimated by counting Fe-rich "reaction" dunites and orthopyroxene-poor harzburgites and lherzolites with wehrlites (hereafter "wehrlite-group peridotites"), compared to "other peridotites" comprising harzburgites and lherzolites with clinopyroxene/orthopyroxene ratios <1. Reaction dunites, with low pyroxene modes, form during open-system processes (*e.g.*, Shaw *et al.*, 2018), whereas here an equilibrium process is modelled. Therefore, reaction dunites and olivine-rich harzburgites with high

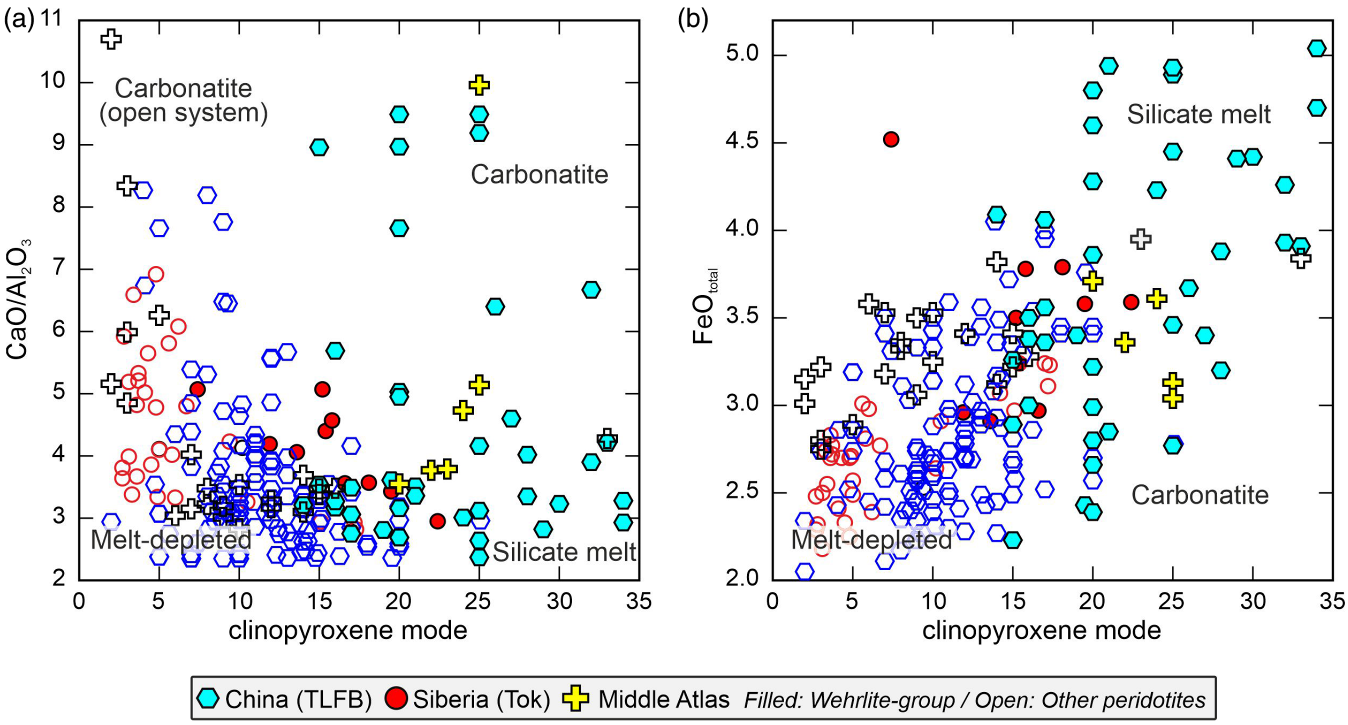

Figure 2 **(a)** CaO/Al_2O_3 and **(b)** FeO_{total} content (wt. %) in clinopyroxene from garnet-free xenoliths as a function of modal abundance (%) of clinopyroxene (Table S-1), illustrating varied effects of wehrlitisation. The type of metasomatic agent is inferred on a suite-by-suite basis from the combined FeO and CaO/Al_2O_3 characteristics of clinopyroxene in wehrlite-group peridotites (Fig. S-2). As an example, for the Tan Lu Fault Belt, wehrlites with clinopyroxene having CaO/Al_2O_3 >6 and FeO <3.5 wt. % are assigned to the carbonatite-metasomatised suite, those with $CaO/Al_2O_3 \leq 6$ and FeO $\geq$ 3.5 wt. % to the silicate melt-metasomatised suite, and the remainder to the carbonated silicate melt-metasomatised suite. Filled symbols denote wehrlite-group peridotites, open symbols denote other peridotites. Orthopyroxene-poor, olivine-rich harzburgites and reaction dunites with low clinopyroxene modes likely interacted with silica-undersaturated melt during open-system processes (Shaw *et al.*, 2018).

clinopyroxene/orthopyroxene ratios are not considered in the calculation of the median clinopyroxene abundance or composition in the wehrlite-group peridotites (Table S-3).

The calculations assume closed-system reactions, resulting in minimum estimates for the volume of silica-undersaturated melt passing through the shallow lithosphere (Yaxley *et al.*, 1998). Because Equation 1 is based on diopside, whereas natural clinopyroxenes are not pure diopside, the difference in median clinopyroxene modes between wehrlite-group and other peridotites is weighted by the median diopside component in clinopyroxene (ΔDi). The mass of enstatite required to produce ΔDi is calculated based on the decarbonation reaction, with two moles of CO_2 liberated *per* mole of diopside formed (Eq. 1). The mass of CO_2 that passed through the shallow lithosphere is estimated by weighting the mass of CO_2 liberated during wehrlitisation by the proportion of wehrlite-group peridotites in each sample suite (Table S-3). The variation of the wehrlite-group proportion in multiple xenolith suites *per* area is taken as the uncertainty. The continental lithospheric area affected by wehrlitisation is estimated using area estimates from the literature or information on the total length of associated rifts, such as the Eastern Rift in the East African Rift and the European Cenozoic Rift System (Supplementary Information). Assuming a density of 3350 kg m^{-3} and a conservative 10 km interval of wehrlitisation, the total mass of liberated CO_2 is estimated. Finally, disequilibrium textures indicate that wehrlitisation occurred close in time to entrainment in the host magma, and that no major fluid- or melt-rock interaction has occurred since. Thus, wehrlitisation and CO_2 degassing are taken to be related to periods of active extension, which facilitates the formation and mobility of small-volume melts (Supplementary Information).

Results and Discussion

In the xenolith suites considered, 6–15 % clinopyroxene was added due to wehrlitisation (Table S-3), corresponding to ΔDi of 3.5 to 12 % and requiring conversion of 6.4 to 22 kg of enstatite (Table 1). Weighted by the proportion of wehrlite-group peridotites in the spinel facies rock column, this amounts to 0.2 ± 0.1 kg (Hoggar Swell) to 2.4 ± 1.5 kg (Eastern Rift) CO_2 *per* 100 kg of wehrlitised peridotite (Table 1). The continental area affected by wehrlitisation ranges from 110×10^3 km^2 (European Cenozoic Rift System) to 4500×10^3 km^2 (Tan Lu Fault Belt). Taking the proportion (and its variability gauged as 1σ) of wehrlite-group peridotites entrained with basalts in each area as representative, this yields total masses of released CO_2 from 24 (±15) × 10^3 Gt to 2100 (±1700) × 10^3 Gt. For estimated timespans of activity from 10 to 40 Myr, this amounts to CO_2 fluxes of 1.4 ± 0.1 Mt yr^{-1} (Pannonian Basin) to 70 ± 58 Mt yr^{-1} (Tan Lu Fault Belt) (Table 1). These estimates indicate significant mantle contributions to the total tectonic and volcanic CO_2 flux at the time of active rifting. For comparison, for conservative flux densities, 40 Mt CO_2 yr^{-1} is estimated for combined present-day active rifts (Brune *et al.*, 2017). Further, amplitudes >80 Mt CO_2 yr^{-1} are estimated for the "Mesozoic CO_2 high", which was associated with a total rift length of 50,000 km (Brune *et al.*, 2017). This suggests that the Tan Lu Fault Belt, which was most active in the Early Cretaceous, was a major contributor to the contemporaneous greenhouse climate. For the Eastern Rift, we obtain ~6.5 ± 4.1 Mt CO_2 yr^{-1} compared to 6–18 Mt CO_2 yr^{-1} attributed to magmatic intrusions into the crust based on surficial CO_2 flux measurements (Hunt *et al.*, 2017). The similar order of magnitude for estimated mantle contributions to CO_2 degassing in the Eastern Rift suggests that wehrlites are well suited to monitor the present and past passage of CO_2 through the shallow lithosphere, which ultimately degassed to the atmosphere. All CO_2 mass estimates are minima because open-system processes (*e.g.*, dunitisation) cannot be quantified using our method. Further, a proportion of clinopyroxene in lherzolites, which were attributed to "other peridotites", may have resulted from wehrlitisation instead. It is also possible that the affected lithospheric depth interval is >10 km (*e.g.*, in the North Atlantic Craton in Greenland it is 20 km; Supplementary Information). Moreover, the width of the affected lithosphere adjacent to rifts may be broader than assumed here.

Modern degassing of mantle-derived CO_2-rich fluids and gases is correlated to active fault systems and extensional tectonic regimes (Brune *et al.*, 2017; Tamburello *et al.*, 2018). A link

Table 1 Modelled loss of CO_2 from spinel peridotite due to wehrlitisation.

Locality	Agent[a]	Area/duration[b]	ΔDi[c]	Enstatite[d]	Dolomite[e]	Perid CO_2 (1σ)[f]	CO_2 flux (1σ)[g]
Unit		1000 km^2/Myr	%	kg	kg	kg	Mt yr^{-1}
Eastern Rift	2	600/40	9.3	20	9.3	2.4 (1.5)	6.5 (4.1)
Aldan Shield	3	200/10	7.1	13	6.1	0.6 (0.4)	4.1 (2.4)
TLFB type 1	1		8.4	16	7.1	0.3 (0.3)	16 (13)
TLFB type 2	2		12	22	10.2	0.3 (0.2)	13 (11)
TLFB type 3	3		9.5	18	8.0	0.8 (0.7)	41 (34)
TLFB combined	1,2,3	4500/30				1.4 (1.2)	70 (58)
Middle Atlas	2	400/40	11	20	9.4	1.5 (0.4)	5.1 (1.2)
Hoggar Swell	3	785/40	3.5	6.4	2.9	0.2 (0.1)	1.5 (0.8)
WEVF	2	110/40	10	19	8.8	1.9 (1.2)	1.7 (1.1)
Pannonian basin	3	133/20	8.7	16	7.4	0.6 (0.1)	1.4 (0.1)

TLFB Tan Lu Fault Belt, WEVF West Eifel Volcanic Field

[a] Type of metasomatic agent involved in wehrlitisation: 1 carbonatite (40–48 wt. % CO_2), 2 carbonated silicate melt (10–30 wt. % CO_2), 3 silica-undersaturated silicate melt (1–5 wt. % CO_2)

[b] Estimated area affected by wehrlitisation and duration of metasomatism/degassing

[c] Difference between median clinopyroxene abundances in wehrlite-group (reaction dunites not counted) and other peridotite xenoliths, weighted by median diopside component (Table S-3)

[d] Mass of enstatite (*per* 100 kg of peridotite converted to wehrlite) required for conversion to mass of diopside corresponding to ΔDi

[e] Mass of dolomite in the liquid (*per* 100 kg of peridotite converted to wehrlite) corresponding to 1/4 of the moles of enstatite as *per* the decarbonation reaction: $4\ MgSiO_3 + CaMg(CO_3)_2 = 2\ Mg_2SiO_4 + CaMgSi_2O_6 + 2\ CO_2$

[f] Mass of CO_2 liberated from 100 kg wehrlite-bearing peridotite using proportion of wehrlite-group peridotites and its variability in Table S-3

[g] Megatonnes CO_2 degassed *per* year for the estimated area and duration (comment b)

between wehrlitisation and extensional settings is also evident in all cases studied here. Tamburello *et al.* (2018) find that current degassing is more prevalent in central Western Europe and the western United States than in cratonic areas. This probably reflects that extension leads to lithosphere thinning, as occurred in the Wyoming Craton and in eastern North China Craton, which hosts part of the Tan Lu Fault Belt. In these settings, oxidised melts collect carbon previously stored in the SCLM (Foley and Fischer, 2017), followed by decarbonation as the melts encounter the solidus ledge of carbonated peridotite (Wallace and Green, 1988). In this case, not only the lithosphere associated with rifts and faults that are recognisable at the surface should be regarded as potential sites of wehrlitisation and CO_2 release, but also lithosphere affected by unsuccessful rifting and thinning, such as the North Atlantic Craton in Greenland, as well as cratonic regions recognised as partially or wholly decratonised (Aulbach, 2019). Moreover, deep lithosphere loss causes lithospheric heating and decompression, as evidenced by microstructural and compositional evidence for garnet breakdown (Supplementary Information). This might not only exhume diamondiferous lithosphere to the shallower mantle where it is oxidised, but also causes crustal metamorphism, which is an important contributor to atmospheric CO_2 (Kerrick, 2001).

Conclusions and Outlook

Wehrlites typically constitute ~20 % of mantle xenolith suites in extensional settings, where continental lithospheres are thinned, facilitating the generation and percolation of small-volume carbonated melts along rifts, faults or in basins. The decarbonation reaction can be applied to wehrlites to estimate the minimum amount of CO_2 that passed through the shallow (~60–100 km) lithosphere. Based on wehrlite-bearing xenolith suites, we calculate CO_2 liberation of 24 ± 15 thousand to 2.1 ± 1.7 million Gt CO_2, with estimated CO_2 fluxes of 1.4 ± 0.1 Mt yr^{-1} to 70 ± 58 Mt yr^{-1}. Ultimate diffuse degassing of this CO_2 is expected to significantly affect climate. Importantly, wehrlitisation may occur wherever continental lithosphere is reactivated, also in lithospheric provinces where prominent rifts are absent and carbonated melts have not been emplaced at the surface. One such example is the basaltic volcanic province of southeastern Australia, where not only the link between wehrlitisation and carbonatite was first established, but also gas fields rich in mantle-derived CO_2 have been connected to the very volcanism that brought the wehrlite xenoliths to the surface (Supplementary Information).

Acknowledgements

This work and collaboration were stimulated by an invitation to SA and GMY to present at the Deep Carbon Observatory's Deep Carbon 2019: Launching the Next Decade of Deep Carbon Science meeting in Washington DC (USA), and by an Alexander von Humboldt Fellowship to GMY, which we gratefully acknowledge. It was written while SA was funded through German Research Foundation fellowship AU356/11. We thank Shantanu Keshav, an anonymous referee as well as the editor, Ambre Luguet, for their very thorough reviews and incisive comments.

Editor: Ambre Luguet

Additional Information

Supplementary Information accompanies this letter at http://www.geochemicalperspectivesletters.org/article2031.

Cite this letter as: Aulbach, S., Lin, A.-B., Weiss, Y., Yaxley, G.M. (2020) Wehrlites from continental mantle monitor the passage and degassing of carbonated melts. *Geochem. Persp. Let.* 15, 30–34.

References

Aulbach, S. (2019) Cratonic Lithosphere Discontinuities: Dynamics of Small-Volume Melting, Meta-Cratonisation and a Possible Role for Brines. In: Yuan, H., Romanowicz, B. (Eds.) *Lithospheric Discontinuities*. American Geophysical Union, John Wiley & Sons, Washington DC, 177–204.

Brune, S., Williams, S.E., Muller, R.D. (2017) Potential links between continental rifting, CO_2 degassing and climate change through time. *Nature Geoscience* 10, 941–946.

Dasgupta, R., Hirschmann, M.M., Smith, N.D. (2007) Partial melting experiments of peridotite CO_2 at 3 GPa and genesis of alkalic ocean island basalts. *Journal of Petrology* 48, 2093–2124.

Foley, S.F., Fischer, T.P. (2017) An essential role for continental rifts and lithosphere in the deep carbon cycle. *Nature Geoscience* 10, 897–902.

Gervasoni, F., Klemme, S., Rohrbach, A., Grützner, T., Berndt, J. (2017) Experimental constraints on mantle metasomatism caused by silicate and carbonate melts. *Lithos* 282–283, 173–186.

Gudfinnsson, G.H., Presnall, D.C. (2005) Continuous gradations among primary carbonatitic, kimberlitic, melilititic, basaltic, picritic, and komatiitic melts in equilibrium with garnet lherzolite at 3-8GPa. *Journal of Petrology* 46, 1645–1659.

Hirschmann, M.M. (2010) Partial melt in the oceanic low velocity zone. *Physics of the Earth and Planetary Interiors* 179, 60–71.

Hunt, J.A., Zafu, A., Mather, T.A., Pyle, D.M., Barry, P.H. (2017) Spatially variable CO_2 degassing in the main Ethiopian rift: implications for magma storage, volatile transport, and rift-related emissions. *Geochemistry Geophysics Geosystems* 18, 3714–3737.

Kerrick, D.M. (2001) Present and past nonanthropogenic CO_2 degassing from the solid Earth. *Reviews of Geophysics* 39, 565–585.

Lin, A.-B., Zheng, J.-P., Aulbach, S., Xiong, Q., Pan, S.-K., Gerdes, A. (2020) Causes and consequences of wehrlitization beneath a trans-lithospheric fault: Evidence from Mesozoic basalt-borne wehrlite xenoliths from the Tan-Lu fault belt, North China Craton. *Journal of Geophysical Research: Solid Earth* 124, e2019JB019084.

Loges, A., Schultze, D., Klügel, A., Lucassen, F. (2019) Phonolitic melt production by carbonatite Mantle metasomatism: evidence from Eger Graben xenoliths. *Contributions to Mineralogy and Petrology* 174, 93.

McKenzie, D. (1989) Some remarks on the movement of small melt fractions in the mantle. *Earth and Planetary Science Letters* 95, 53–72.

Rohrbach, A., Schmidt, M.W. (2011) Redox freezing and melting in the Earth's deep mantle resulting from carbon-iron redox coupling. *Nature* 472, 209–212.

Shaw, C.S.J., Lebert, B.S., Woodland, A.B. (2018) Thermodynamic Modelling of Mantle–Melt Interaction Evidenced by Veined Wehrlite Xenoliths from the Rockeskyllerkopf Volcanic Complex, West Eifel Volcanic Field, Germany. *Journal of Petrology* 59, 59–86.

Tamburello, G., Pondrelli, S., Chiodini, G., Rouwet, D. (2018) Global-scale control of extensional tectonics on CO_2 earth degassing. *Nature Communications* 9, 4608.

Wallace, M.E., Green, D.H. (1988) An experimental determination of primary carbonatite magma composition. *Nature* 335, 343–346.

Yaxley, G.M., Green, D.H. (1996) Experimental reconstruction of sodic dolomitic carbonatite melts from metasomatised lithosphere. *Contributions to Mineralogy and Petrology* 124, 359–369.

Yaxley, G.M., Green, D.H., Kamenetsky, V. (1998) Carbonatite metasomatism in the southeastern Australian lithosphere. *Journal of Petrology* 39, 1917–1930.

Geochemical Perspectives Letters

Wehrlites from continental mantle monitor the passage and degassing of carbonated melts

S. Aulbach, A-Bing Lin, Y. Weiss, G.M. Yaxley

Supplementary Information

The Supplementary Information includes:

- Oxygen Fugacity Control on Redox Freezing *vs.* Wehrlitisation during Interaction with Carbonated Melts
- Compositional Effects of Wehrlitisation and the Role of Lithosphere Thickness
- Selection Criteria, and Assignation to Wehrlite-group Peridotites
- Wehrlite-bearing Xenolith Suites and their Tectonic Setting
- CO_2 Liberation during Wehrlitisation: Modelling and Rationale
- Figures S-1 to S-3
- Tables S-1 to S-3
- Supplementary Information References

Oxygen Fugacity Control on Redox Freezing vs. Wehrlitisation during Interaction with Carbonated Melts

The low proportion of wehrlite amongst garnet peridotites and inclusion-bearing diamonds is striking (Fig. S-1a,b) when compared against the proportion of wehrlite in spinel peridotite xenoliths in this study (Table S-3). This can be explained by the effect of oxygen fugacity (fO_2) on the stabilisation of carbonate/carbonated melt vs. graphite/diamond. Garnet and diamond are only stable at high pressures ≥~2 and ~3.5 GPa, depending on composition and the geothermal gradient to which their host rock equilibrated. The vast majority of garnet peridotite investigated to date have fO_2 relative to the Fayalite-Magnetite-Quartz (FMQ) buffer ≤ -1 (*e.g.*, Woodland and Koch, 2003; Yaxley *et al.*, 2017). However, solid carbonate or pure carbonatite melt are only stable at FMQ ≥ -1.5 to -1, depending on pressure (Stagno *et al.*, 2013). Carbonated silicate melts, which are stable to lower fO_2 precipitate graphite/diamond according to the reaction:

$$4\,FeO + CO_2 = 2\,Fe_2O_3 + C \quad \text{(Eq. S-1)}$$

which has been referred to as “redox freezing” (Rohrbach and Schmidt, 2011). Since fO_2 increases with decreasing pressure in the mantle lithosphere (*e.g.*, Woodland and Koch, 2003), pure carbonatite or carbonated silicate melt may be stable in the spinel peridotite facies. This may explain the higher abundances of wehrlite xenoliths at locations affected by extension.

Compositional Effects of Wehrlitisation and the Role of Lithosphere Thickness

The presence of a thick lithospheric lid, typically in intact cratons, impedes decompression melting, allowing no or only small-volume melts to be stabilised as a function of temperature, composition and fO_2 (*e.g.*, Aulbach, 2019). In contrast, thinner lithospheres allow longer melting columns to be established, with stronger dilution of the melt with silicate components (*e.g.*, Stamm and Schmidt, 2017). Consequently, disrupted cratons, the deep roots of which are thermally and compositionally strongly overprinted, and metacratons, the deep roots of which have been lost altogether, are typically associated with magmatism involving higher-volume melt (*e.g.*, Aulbach, 2019). Microstructures associated with garnet breakdown are described for some wehrlite-bearing xenolith suites (reviewed below), which suggests decompression to the spinel stability field in the context of extension and lithosphere thinning. Dilution with silicate components during sustained decompression melting entails higher contents of "basaltic" components in the melt, such as Al_2O_3 and FeO. Clinopyroxene in wehrlites from Greenland are characterised by low TiO_2 and FeO, but strongly elevated CaO/Al_2O_3 commonly ascribed to interaction with a carbonatite melt (Aulbach *et al.*, 2017), whereas those from Tok have high FeO and Al_2O_3 and in part TiO_2 contents, which are explained by reaction with silicate melt (Ionov *et al.*, 2005a) (Fig. S-2). Wehrlite-bearing xenolith suites from other localities show intermediate compositions (East African Rift, West Eifel Volcanic Field), which have been ascribed to carbonatites (Rudnick *et al.*, 1993) and alkaline mafic melts (Shaw *et al*., 2018), respectively. For the purpose of inferring the metasomatic agent based on reported clinopyroxene composition (Fig. S-2), we only consider garnet-free peridotites because the presence of garnet affects Al_2O_3 and Y-HREE partitioning into clinopyroxene, which we use to infer the metasomatic agent involved in wehrlitisation. This garnet effect is illustrated for trace elements in Figure S-3.

Interaction of mantle peridotite with carbonatite and silicate melt leads to a distinct minor- and trace-element relationships in the clinopyroxene: LREE tend to be strongly enriched over HREE in carbonatite-metasomatised peridotite while Ti is not enriched along with MREE, whereas the opposite results from interaction with silicate melt (*e.g.*, Yaxley *et al.*, 1991; Rudnick *et al.*, 1993; Coltorti *et al.*, 1999) (Fig. S-3). Elevated La/Gd, Ce/Yb and Pr and low Ti/Eu and Y result from interaction with carbonatite and/or with a melt that has percolated garnet-bearing mantle (Fig. S-3). Prior depletion related to partial melt extraction during stabilisation of the lithosphere is evident in low absolute Pr abundances. Thus, abundances of strongly incompatible elements decrease and of less incompatible elements increase with increasing volume of the metasomatic melt, and this signature is imposed on the metasomatised mantle volume. These systematics are also observed in clinopyroxene from peridotites other than wehrlite-group peridotites because cryptic metasomatism affects the incompatible element budget without changes in major element content and mineralogy (Dawson, 1984). In addition to this first-order effect of melt volume, the nature of the wall-rock with which the melt has interacted *en route* to the site of wehrlitisation strongly affects the compositional signature. For example, a kimberlite-like melt that extensively reacted with garnet-bearing mantle becomes increasingly Y- and HREE-poor and incompatible element-enriched (Aulbach *et al.*, 2013). When garnet-bearing mantle is absent, such melts have higher Y and La/Gd closer to the primitive mantle (Fig. S-3). Due to effects of lithosphere thickness, there is no single major- or trace-element characteristic associated with wehrlitisation.

Selection Criteria, and Assignation to Wehrlite-group Peridotites

Localities were chosen (1) that are considered representative with respect to tectonic settings (on- and off-craton, rift and basin), (2) for which the necessary data have been published that allow calculation of the CO_2 released during wehrlitisation (mineral modal abundances, clinopyroxene major-element compositions). Additional studies on wehrlite-bearing xenolith suites are available, but some are compositionally unequilibrated, precluding the use of average compositions or determination of mineral modes (*e.g.*, Eastern Australia: Yaxley *et al.*, 1991, 1998; Eger Graben: Loges *et al.*, 2019; Hoggar Swell: Kaczmarek *et al.*, 2016). Others are garnet-bearing (*e.g.*, Kimberley; Rehfeldt *et al.*, 2008), which complicates the interpretation of the metasomatic signatures as outlined in the previous section. Moreover, as ≤ 1% of garnets from the garnet and diamond-stable lithosphere are wehrlitic (Fig. S-2), they are not further considered here.

The wehrlites under consideration formed as a result of mantle metasomatism rather than accumulation from silica-undersaturated melt, such as those reported from the Wyoming Craton (Downes *et al*., 2004), and sometimes both types are present in a xenolith suite (*e.g.*, in the West Eifel Volcanic Field: Zinngrebe and Foley, 1995; East

African Rift: Davies and Lloyd, 1989). These two possibilities can be distinguished based on texture (sieved-textured clinopyroxene, absence of cumulate microstructures, textures showing replacement of orthopyroxene by clinopyroxene) and chemical composition (Na_2O in clinopyroxene >0.8 wt%, olivine Mg# >0.84; incompatible-element enrichment) (Lin et al., 2020).

A common classification scheme for ultramafic rocks is that by Streckeisen (1976), where peridotites with >40% olivine and <5% orthopyroxene are classified as wehrlites, whereas harzburgites with <5% clinopyroxene are produced by melt extraction from lherzolite. Melting reactions for spinel peridotite almost invariably indicate that clinopyroxene and orthopyroxene are consumed at a clinopyroxene/orthopyroxene ratio >1 (Walter, 2014). This produces olivine up to pressures of ~1.7 GPa, above which orthopyroxene may be produced, with estimates for clinopyroxene modes in the primitive mantle from 17 to 20% (Walter, 2014). Therefore, in melt residues, orthopyroxene/clinopyroxene ratios should be >1, whereas ratios <1 and clinopyroxene modes ≥20% may reflect wehrlitisation. Thus, clinopyroxene-rich, orthopyroxene-poor xenolith varieties that are classified as lherzolites according to Streckeisen (1976) were plausibly affected by the wehrlitisation process. In some xenolith suites, reaction dunites showing evidence for recent orthopyroxene-breakdown have major- and trace-element characteristics similar to wehrlites (*e.g.*, Mg# < olivine in primitive mantle) (*e.g.*, North Atlantic Craton in SW Greenland; Aulbach *et al.*, 2017). Such dunites are distinct from refractory melt extraction residues. They may form in channels preceded by reactive porous flow, as suggested for Fe-rich wehrlites (Raffone *et al.*, 2009), and they are here regarded as the (end) products of wehrlitisation under open-system conditions. As defined in the main text, wehrlite-group peridotites encompass Fe-rich "reaction" dunites, and orthopyroxene-poor lherzolites and harzburgites in addition to wehrlites.

Wehrlite-bearing Xenolith Suites and their Tectonic Setting

East African Rift (EAR), Tanzanian craton (disrupted)

Development of the EAR is associated with the Oligocene arrival of the Afar plume that caused widespread lithosphere thinning (Furman et al., 2016). The EAR stretches for some 6,000 km from north to south (Chorowicz, 2005). Samples from the Pleistocene Olmani and Labait cinder cones at and near the Tanzanian craton margin in the EAR comprise a total of 32 garnet-free peridotite xenoliths (Jones *et al.*, 1983; Rudnick *et al.*, 1993, 1994; Lee and Rudnick, 1999). 78 and 30%, respectively, of the garnet-free peridotite samples at these localities are wehrlites and reaction dunites (*i.e.* wehrlite-group peridotites; Table S-3). The latter show increased FeO, but inconspicuous Al_2O_3, CaO and TiO_2. Garnet-bearing peridotites also occur at Labait. Unusually low Al_2O_3 and high Ca/Al in clinopyroxene, the occurrence of monazite and apatite in some peridotites, as well as elevated Zr/Hf in peridotites from Olmani have been ascribed to carbonatite metasomatism (Rudnick *et al.*, 1993). Spinel peridotites from Labait, located at ~70 to 130 km depths record fO_2 of FMQ-0.5 to FMQ+0.4, *i.e.* they are oxidising relative to the Kaapvaal or Siberian craton at similar depth (Zhang *et al.*, 2017). A pre-entrainment enrichment event is recognised based on Li elemental and isotope systematics (Aulbach and Rudnick, 2009). Mid-lithospheric discontinuities related to melt metasomatism are detected at 60 to 100 km depth in the western craton (Wölbern *et al.*, 2012). The lithosphere-asthenosphere boundary (LAB) in the craton is at 150 to 200 km depth (Weeraratne *et al.*, 2003).

Tok, Aldan Shield, Siberian craton (disrupted)

Peridotite xenoliths from the Quaternary Tok volcanic field in the Aldan Shield at the SE Siberian craton margin were investigated by Ionov *et al.* (2005a,b, 2006). They comprise refractory, metasomatised lherzolites and wehrlites with elevated Ca, Fe and Ti contents (Fig. S-2), which have been ascribed to interaction with silica-undersaturated, alkali-rich silicate melt (Ionov *et al.*, 2005a). 21% of 48 xenoliths are wehrlites and orthopyroxene-poor lherzolites (Table S-1). The metasomatic agent ultimately formed from an underplated and fractionated basic melt, whereby carbonate-rich derivatives caused the strongest enrichments (Ionov *et al.*, 2006). Oxygen fugacities have not been reported for this mantle section. The Aldan shield was in an extensional regime in the early Cretaceous, with emplacement of alkaline rocks linked to the nearby Transbaikalian rift (Ivanov *et al.*, 2018). The Baikal rift, with a total of 2,000 km *en echelon* rift depressions (Tiberi *et al.*, 2003), records initial Late Cretaceous extension and increased activity in the Late Miocene to Early Pliocene, associated with subduction of the Pacific plate (Jolivet *et al.*, 2009). The associated lithospheric disruption resulted in reduced depth to the LAB (~140-190 km; Artemieva, 2006) compared to the intact Siberian craton (200 to 250 km; Priestley and Debayle, 2003).

North Atlantic Craton in SW Greenland (GNAC) (disrupted)

Forty-two metasomatised peridotite xenoliths from the Mesozoic Pyramidefjeld and Midternaes kimberlite comprise garnet-free lherzolites, harzburgites and reaction dunites from 100 to 170 km depth, and texturally equilibrated reaction dunites and olivine-rich phlogopite-bearing wehrlites from 90 to 110 km depth (Aulbach *et al.*, 2017) (Table S-1). Based on microstructural evidence for garnet break-down, the metasomatic overprint may be linked to the latest, Mesozoic, rifting event, which was preceded by multiple failed rifting episodes and accompanied by partial destruction of the lithospheric mantle (Tappe *et al.*, 2012). The intense metasomatism is proposed to have been oxidising based on the less compatible behaviour of V in wehrlites compared to other peridotites (Aulbach *et al.*, 2017). The high olivine modes also in the wehrlites (>80%) suggest an open-system process that precludes calculation of CO_2 fluxes through the lithosphere. The 20 km depth interval at 90 to 110 km appears to be nearly completely converted to wehrlite and related rocks (only one of 17 samples is lherzolite). Wehrlitic clinopyroxenes are characterised by very high CaO/Al_2O_3 (Fig. S-2), whereas trace elements in part show the influence of the garnet-bearing deeper lithosphere (Figs. S-3) (Aulbach *et al.*, 2017). Wehrlites and related rocks spatially overlap a seismically detected discontinuity with a negative phase (Kumar *et al.*, 2005). Garnet peridotites with equilibration pressures of up to 5.5 GPa (Nielsen *et al.*, 2008) indicate a minimum depth to the LAB of ~170 km, and a depth of ~210 km is seismically determined (Artemieva, 2019).

Tan Lu Fault Belt (TLFB), NE China (including decratonised North China Craton)

The TLFB experienced sinistral strike-slip in the earliest Cretaceous, followed by a brief period of compression and a long period of extension in the Early Cretaceous, related to subduction, slab roll-back and back-arc extension of the Palaeo-Pacific plate (Zhu *et al.*, 2018). Its total length and width are 5,000 × 800 to 1,000 km (Xu *et al.*, 1987). Numerous well-studied mantle xenolith suites comprising a high proportion of wehrlites were entrained during Late Cretaceous (Liaoyuan) to Cenozoic (Beiyan, Liaoyuan, Nushan, Shanwang, Yitong) alkaline magmatism (Table S-1). The wehrlites formed by interaction with silica-undersaturated CO_2-H_2O-bearing melts, based also on the presence, or evidence for the former presence, of amphibole (Lin *et al.*, 2020, and references therein). Signatures of wehrlitisation along the fault vary. Based on CaO-Al_2O_3-FeO relationships observed in clinopyroxene (Fig. S-2) 15 of 60 samples are inferred to have reacted with a carbonatite, nine with a carbonated silicate melt and the majority (n = 36) with a silica-undersaturated silicate melt (Table S-3). The proportion of wehrlites at each locality varies from none at Nushan to 75% at Liaoyuan (36 ± 30 1σ). Peridotites along the TLFB record oxygen fugacities of FMQ-2 to FMQ+0.8 at pressures of 1 to 2 GPa (Lin *et al*., 2020, and references therein). Regional oxidation and hydration, via influx of fluids sourced from the Palaeo-Pacific plate, may have remobilised CO_2 stored in the lithosphere by lowering the peridotite solidus (Geng et al., 2019). Development of the TLFB temporally overlaps the Mesozoic loss of the diamondiferous mantle root beneath the eastern North China craton (NCC) (Zhu *et al.*, 2018). Decratonization of the eastern NCC has been linked to seismic velocity reductions at 80 to 120 depth in the intact western NCC, which are interpreted as weak zones that were present also beneath the eastern NCC before the Mesozoic decratonisation (Chen *et al.*, 2014).

Middle Atlas, Morocco, NW Africa (reactivated Pan-African basement)

Late Pliocene to Quarternary alkaline volcanism (alkali basalts, basanites, nephelinites) in the Pan-African basement of the Middle Atlas is associated with the Trans-Moroccan fault system and entrained a diverse xenolith suite with variable amphibole contents (Raffone *et al.*, 2009). This suite, which records fO_2 of FMQ-0.1 to FMQ+1.8, comprises ~24% wehrlites that formed through interaction with alkaline melts (Fe-wehrlites) and subordinately carbonatite or highly evolved melts (Mg-wehrlites) (Raffone *et al.*, 2009) (Table S-1). One wehrlite and two clinopyroxene-rich lherzolites with clinopyroxene/orthopyroxene ratios of 1.7 (43%) out of seven peridotite xenoliths from the Azrou-Timahdite region are reported in Chanouan *et al*. (2017), confirming a high proportion of mantle affected by silica-undersaturated melt-metasomatism. Metasomatism is thought to have occurred in the Late Cretaceous or Eocene during tectonic reactivation (Raffone *et al.*, 2009; Wittig *et al.*, 2010). Reaction patches with secondary clinopyroxene and olivine, ascribed to interaction with asthenospheric alkali silicate melts, are reported for spinel lherzolites entrained in basalts some 1,500 km southeast, in Gharyan, Libya (Beccaluva *et al.*, 2008). These authors suggest that the Cenozoic volcanism in NW Africa reflects lithosphere rejuvenation and rifting within the Pan-African (or older) basement in reaction to the collision of the African and European plates.

Hoggar Swell, Algeria, NW Africa (reactivated Pan-African basement)

Some 1,000 km to the SSE of the Middle Atlas, in the Hoggar Swell, xenoliths from Neogene to Quarternary basanites and nephelinites show evidence for metasomatism by highly alkaline silicate melts to carbonate melts derived from the asthenosphere or rejuvenated lithosphere (Dautria *et al.*, 1992; Beccaluva *et al.*, 2007; Kourim *et al.*, 2014; Kaczmarek *et al.*, 2016). Kourim *et al.* (2014) report petrographic data for 28 peridotite xenoliths from the Tahalgha District, of which 7 are wehrlites (5 amphibole-bearing) (25%). Of 22 texturally heterogeneous samples from In Teria (Kaczmarek *et al.*, 2016), two are wehrlites and one is an olivine clinopyroxenite, as grouped together by the authors (14%) (Table S-1). There is evidence for the re-equilibration of spinel lherzolites from garnet-bearing mantle domains, which testifies to decompression (Beccaluva *et al.*, 2007). Rare garnet peridotites reported from other localities are interpreted as the relics of an original thicker lithosphere (Kaczmarek *et al.*, 2016). The Hoggar Swell adjoins the Saharan "metacraton" (500,000 km^2), which is transected by multiple megafaults and has a lithosphere thickness of ~100 to 150 km, compared to the adjacent West African craton with up to 250 km thickness (Liégeois *et al.*, 2003; Abdelsalam *et al.*, 2011). The intervening decratonised lithosphere underlying the Pan-African Swell, with a diameter of ~1,000 km (Liégeois *et al.*, 2005), is similarly vast.

West Eifel Volcanic Field (WEVF), Germany (off-craton)

The <1 Myr WEVF is located between the Upper and Lower Rhine Graben (part of the European Cenozoic Rift System (ECRS), with a total length of ~1,100 km; Ziegler and Dèzes, 2005). It belongs to the Central European Volcanic Province (Trieloff and Altherr, 2007). The underlying mantle is heterogeneous, with an abundance of wehrlites and orthopyroxene-poor harzburgites (Table S-1). Micaceous hornblendite veins in composite xenoliths attest to the action of hydrous melts before entrainment, whereas strongly LREE-enriched clinopyroxenes in the vein-hosting peridotite require earlier metasomatism (Witt-Eickschen *et al.*, 1998). Wehrlite and orthopyroxene-poor harzburgites (n = 4; 12%), of which one adjacent to a hornblendite vein, are described amongst 33 xenoliths from Dreiser Weiher, Meerfelder Maar and other localities, including two samples from the East Eifel (Witt-Eikschen *et al.*, 1998; 2003; Witt-Eickschen and O'Neill, 2005). Zinngrebe and Foley (1995) describe a suite of xenoliths from Gees with an abundance of wehrlites and clinopyroxene-dunites (n = 13; 68%) relative to other peridotites (n = 6). Abundant glass and unequilibrated textures preclude modal estimates. Twenty spinel peridotites from the Rockeskyllerkopf comprise 55% wehrlites and reaction dunites with abundant phlogopite and minor amphibole (not counting phlogopite-clinopyroxene veins), which were metasomatised by a silica-undersaturated alkaline melt before Quaternary magmatism (Shaw *et al.*, 2018). Witt-Eikschen and O'Neill (2005) obtain FMQ-0.2 ± 0.5 based on mineral equilibria. Diffusion modelling indicates that metasomatism occurred within <1 Myr of entrainment (Shaw *et al.*, 2018). Noble gas isotope systematics in mantle xenoliths from the WEVF and Pannonian Basin suggest that CO_2-rich fluids were trapped during mantle metasomatism from lithospheric and plume-derived sources (Trieloff and Altherr, 2007). Regional lithospheric thickness ranges from 50 to 120 km, after reworking of an originally thicker Variscan root (Ziegler and Dèzes, 2005). The ECRS was activated in the Late Eocene, by compression resulting from Alpine Pyrenean collision zones (Dèzes *et al.*, 2004).

Pannonian Basin, Hungary (off-craton)

The Pannonian Basin, wedged between the Alpine, Dinaride and Carpathian orogenic belts, experienced Early Miocene passive rifting with the formation of an extensional back-arc basin, followed by Late Miocene asthenospheric upwelling and active thinning in the central basin (Szabó *et al.*, 2004). Mantle xenoliths entrained in Neogene alkali basalts provide evidence for the reaction of the lithospheric mantle with carbonated melts. This includes direct observations of CO_2-bearing glass pockets in a wehrlite-bearing suite dominated by lherzolite and harzburgite, part of which show evidence for orthopyroxene break-down (Créon *et al.*, 2017). Modal abundances are not reported. Furthermore, CO_2-rich fluid inclusions with negative crystal shapes in clinopyroxene occur in lherzolites and harzburgites described by Berkesi *et al.* (2012). Two of nine xenoliths (22%) in their study are olivine-rich (>81.7% olivine) and orthopyroxene-poor (≤11.1 % orthopyroxene), and are assigned here to the wehrlite-group peridotites. Abundant wehrlite xenoliths (24% of 63 samples) entrained from ~1.2 to 1.6 GPa are found in the central part of the Nógrád-Gömör Volcanic Field in the northern Pannonian Basin (Patkó *et al.*, 2013, 2020; Liptai *et al.*, 2017) (Table S-1). Wehrlitisation occurred via interaction with a silicate melt similar to the host basalt, leading to increased Fe, Ti, Ca and Al contents and formation of amphibole (Patkó *et al.*, 2020). Lherzolites record fO_2 of FMQ-0.8 ± 0.7 (Patkó *et al.*, 2019). Of 22 samples entrained in Pliocene basalt from Balaton, some 200 km southwest (Ntaflos *et al.*, 2017), one clinopyroxene-rich dunite and one orthopyroxene-poor lherzolite (9%) appear to have interacted with silica-undersaturated melt. In the eastern basin, refertilisation by Carpathian-Pannonian-type subduction-related silicic melts preceded an alkaline event (Faccini et al., 2020), making it difficult to disentangle the effects of the latter, and this locality is therefore not considered here. Garnet breakdown products observed in some mantle xenoliths (Szabó *et al.*, 2004) suggest extension-related decompression of originally thicker lithosphere. The depth of the LAB is estimated at 70 to 100 km (Alasonati Tasárova *et al.*, 2016).

Southeastern Australia (off-craton)

Wehrlite xenoliths from SE Australia are compositionally unequilibrated (*e.g.*, Yaxley *et al.* 1991, 1998), precluding their use to estimate CO_2 flux described in the next section. Nevertheless, a more detailed description is provided here because the wehrlitisation reaction involving carbonatite was originally described in xenoliths from Victoria in southeastern Australia (Green and Wallace, 1988). Late Cretaceous to Holocene intraplate basaltic volcanism was widespread in SE Australia, and has been linked to the breakup of Gondwana and rifting of the Australian plate, followed by edge-driven convection that facilitated decompression melting (Oostingh *et al.*, 2016). The volcanics were emplaced into the Lachlan and Delamerian Fold Belts, which are crossed by a series of north-south-trending faults (Oostingh *et al.*, 2016), but a continent-scale rift or basin are absent. The faults currently provide pathways for predominantly mantle-derived CO_2 in SE Australian gas fields (Karolyte *et al.*, 2019). This is sampled in CO_2 springs, which are abundant in the Central Victorian Highlands, and in gas wells in the Otway Basin to the south (Karolyte *et al.*, 2019). The mantle CO_2 has been related to Pliocene to Recent basalts of the Newer Volcanic Province (Cartwright *et al.*, 2002), in which wehrlite-bearing xenolith suites occur.

CO_2 Liberation during Wehrlitisation: Modelling and Rationale

For the purpose of modelling the mass of CO_2 liberated during wehrlitisation, we consider only garnet-free and spinel peridotites, which sample the shallow mantle lithosphere where the decarbonation reaction takes place (Wallace and Green, 1988). Individual xenoliths with key characteristics are listed in Table S-1, key median compositions are shown in Table S-3. Based on the decarbonation reaction (main text), we calculate the mass of enstatite required to generate the additional diopside formed due to wehrlitisation (*i.e.* the difference between median clinopyroxene modes in wehrlite-group and "other peridotites", weighted by median diopside component). No adjustment is made for modal abundances reported as weight vs. volume fractions, but for rocks dominated by mantle olivine and pyroxenes with similar densities (see, *e.g.*, Lee, 2003), the effect is minor (*e.g.*, 10.1 wt% clinopyroxene correspond to 10.0 vol.%) relative to uncertainties in the CO_2 degassing modelling. According to the reaction, the molar abundance of CO_2 liberated corresponds to ½ that of enstatite. This is then converted to mass of CO_2 liberated per 100 kg of wehrlitised peridotite and finally weighted by the proportion of wehrlite-group peridotites to calculate the mass of CO_2 liberated per 100 kg of peridotite in the lithosphere column. This result is independent of the CO_2 content in the metasomatic agent. For increasingly SiO_2-rich and correspondingly CO_2-poor liquids (corresponding to increasing melt fractions) higher volumes of melt, hence melt-rock ratios, are required to convert orthopyroxene to clinopyroxene. The likely metasomatic agent is inferred from the combined FeO and CaO/Al_2O_3 characteristics of wehrlites, which is evaluated on a suite-by-suite basis (Fig. S-2). As an example, for the TLFB, wehrlites with CaO/Al_2O_3 >6 and FeO <3.5 wt% are assigned to the carbonatite-metasomatised suite, those with CaO/Al_2O_3 ≤6 and FeO ≥ 3.5 wt% to the silicate melt-metasomatised suite, and the remainder to the carbonated silicate melt-metasomatised suite.

To calculate the total mass of CO_2 liberated, it is necessary to estimate the area and depth interval of lithosphere that was affected. Pressures for spinel peridotites are difficult to estimate accurately. We here conservatively assume that a 10 km lithosphere depth interval has been converted to wehrlite. Furthermore, we assume that xenolith localities sampling a portion of a rift system, continental-scale fault system or basin are representative of the entire system. Areal estimates are available for the Hoggar Swell (~785,000 km^2; Liégeois *et al.*, 2005), the Pannonian Basin (133,000 km^2) and the TLFB (4,500,000 km^2; Xu *et al.*, 1987, assuming a median width of 900 km). Brune *et al.* (2017) suggest, as a minimum, that rifts are 50 km wide. We use double this estimate because small-volume melt magmatism occurs on the shoulders of currently active rifts, such as the EAR, whereas this type of magmatism has been superseded by higher-volume basaltic melts in the rift itself (Foley and Fischer, 2017). For the 3250 km long Eastern Rift (Hunt *et al.*, 2017), this yields an area of 325,000 km^2, for the 2000 km long greater Baikal and Transbaikal rifted region 200,000 km^2 and for the 1100 km long ECRS (Ziegler and Dèzes, 2005) 110,000 km^2. Based on Figure 1 in Liégeois et al. (2005), the entire length and width of the area encompassing the Middle Atlas and

Gharyan in NW Africa are estimated at 2000 × 200 km, respectively.

To estimate the carbon flux, the duration of CO_2 liberation must be known. For the TLFB, Zhu *et al.* (2018) suggest a major extensional period in the Early Cretaceous following compression in the earliest Cretaceous and followed again by compression before the end of the Early Cretaceous, which is here taken to correspond to ca. 30 Ma. Although xenolith-bearing basalts along the TLFB are mainly Cenozoic, abundant wehrlites in the Late Cretaceous Liaoyuan basalts suggest a temporal link of wehrlitisation to main rift activity. Miocene passive to active rifting in the Pannonian Basin (Szabó *et al.*, 2004) translates to some 20 Ma of activity. Foley and Fischer (2017) estimate a 40 Ma lifespan for continental rifts, which is applied to the EAR. Activation of the ECRS in the Late Eocene (Dèzes *et al.*, 2004) may imply some 40 Ma of activity until today. Taking increased activity in the Late Miocene to Early Pliocene in the greater Baikal and Transbaikal rifted region (Jolivet *et al.*, 2009), we estimate a duration of 10 Ma. Based on isotopic compositions of xenoliths from the Hoggar Swell, metasomatism has been estimated to have occurred no earlier than 40 Ma prior to eruption. This timespan is adopted here for the Hoggar Swell and also the Middle Atlas, where magmatism and pre-entrainment metasomatic evolution has been linked to rifting of the Pan-African basement (Raffone *et al.*, 2009).

Supplementary Tables

Table S-1 Rock types, clinopyroxene modes and compositions for wehrlite-bearing xenolith suites from various localities, and clinopyroxene associated with carbonatitic high-density fluids in diamond (Excel file available for download from the online version of the article at http://www.geochemicalperspectivesletters.org/article2031).

Table S-2 List and salient compositions (wt. %) of high-density fluids in diamond and of experimentally produced liquids (Excel file available for download from the online version of the article at http://www.geochemicalperspectivesletters.org/article2031).

Table S-3 List and salient median compositions of clinopyroxene in wehrlite-bearing xenolith suites.

Locality/lithology	n	% wehr (1σ)	cpx mode %	FeO^{total} wt. %	CaO/Al_2O_3	Di mol
Labait and Olmani, Tanzanian Craton margin (disrupted), East African Rift						
Wehrlite-group	14	54 (34)	14	3.9	15.3	0.80
Other peridotites	18		3	2.7	9.2	0.76
Tok, Siberian Craton margin (disrupted), Aldan Shield						
Wehrlite-group	10	21 (20)	16	3.6	3.8	0.67
Other peridotites	37		5	2.7	4.1	0.68
Pyramidefjeld and Midternaes, North Atlantic Craton (NAC, disrupted) in SW Greenland						
Wehrlite-group	9	na	na	2.5	83.1	0.87
Other peridotites	15	na	na	3.1	9.5	0.78
Tan Lu Fault Belt, NE China (including decratonised North China Craton)						
Wehrlite - type 1	15		20	2.7	12.2	0.81
Wehrlite - type 2	9	36 (30)	25	4.9	9.2	0.78
Wehrlite - type 3	36		23	3.9	3.3	0.71
Other peridotites	156		11	2.8	3.1	0.69
Middle Atlas, Morocco, rifted Pan-African basement						
Wehrlite-group	7	34 (8)	24	3.6	4.3	0.70
Other peridotites	23		9	3.3	3.5	0.69
Hoggar Swell, Algeria, rifted Pan-African basement						
Wehrlite-group	7	16 (9)	18	4.9	3.3	0.66
Other peridotites	21		12	3.5	3.3	0.70
West Eifel Volcanic Field, Shoulder Rhine Graben, European Cenozoic Rift System (off-craton)						
Wehrlite-group	15	45 (29)	18	3.1	7.3	0.78
Other peridotites	38		5	2.7	4.4	0.75
Nógrád- Gömör+Bakony-Balaton, Pannonian Basin, Cenozoic European Basin System (off-craton)						
Wehrlite-group	19	18 (8)	21	4.0	4.1	0.70
Other peridotites	76		8	2.8	3.8	0.71

n number of samples (Table S-1), *% wehr (1σ)* average percentage of wehrlite-group peridotites in multiple xenolith suites and one standard deviation; average standard deviation from all other estimates is used for Tok, where wehrlite percentage is available from only one locality; *cpx mode* clinopyroxene modal abundance, *Di mole* diopside mole fraction in clinopyroxene; wehrlite-group includes wehrlite, orthopyroxene-poor lherzolite and harzburgite and reaction dunite, other peridotites includes harzburgites and lherzolites; type refers to wehrlitising agent as defined in Table 1; individual samples with references in Table S-1, further details in Supplementary Information.

Supplementary Figures

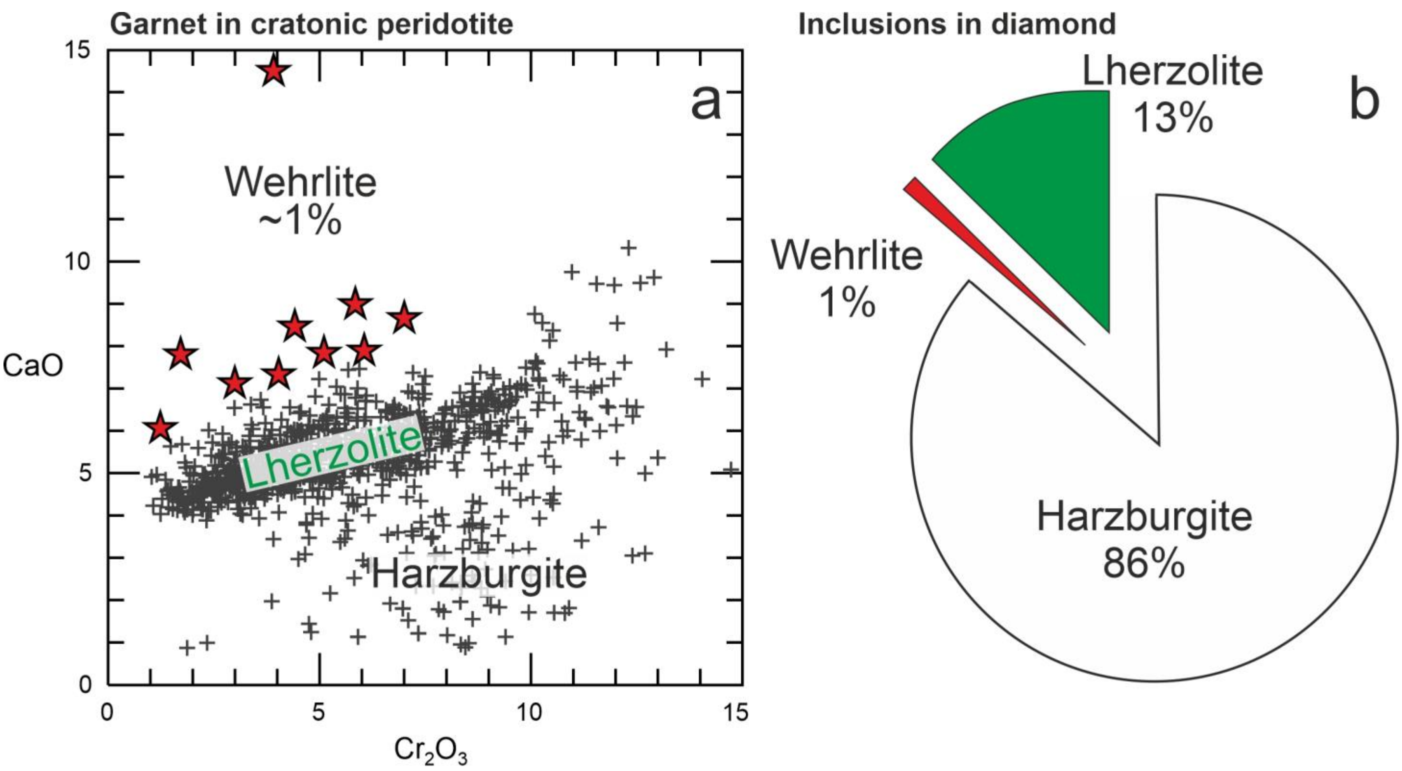

Figure S-1 **(a)** Wehrlitic garnet (red stars) and garnet in other peridotites (crosses) in >950 cratonic peridotite xenoliths (Boyd, 1974; Ehrenberg, 1982; Mitchell, 1984; Danchin and Boyd, 1976; Sobolev *et al.*, 1984; Hervig *et al.*, 1986; Winterburn *et al.*, 1990; Viljoen, 1994; Franz *et al.*, 1996; Boyd *et al.*, 1997; Stachel *et al.*, 1998; Kopylova *et al.*, 1999; MacKenzie and Canil, 1999; Schmidberger and Francis, 2001; Hearn, 2004; Kopylova and Caro, 2004; Menzies *et al.*, 2004; Grégoire *et al.*, 2005; Westerlund *et al.*, 2006; Aulbach *et al.*, 2007; Simon *et al.*, 2007; Creighton *et al.*, 2008, 2010; Hin *et al.*, 2009; Ionov *et al.*, 2010; Ivanic *et al.*, 2012), using the classification scheme of Grütter *et al*. (2004). **(b)** Parageneses of inclusions in diamond (Stachel and Harris, 2008).

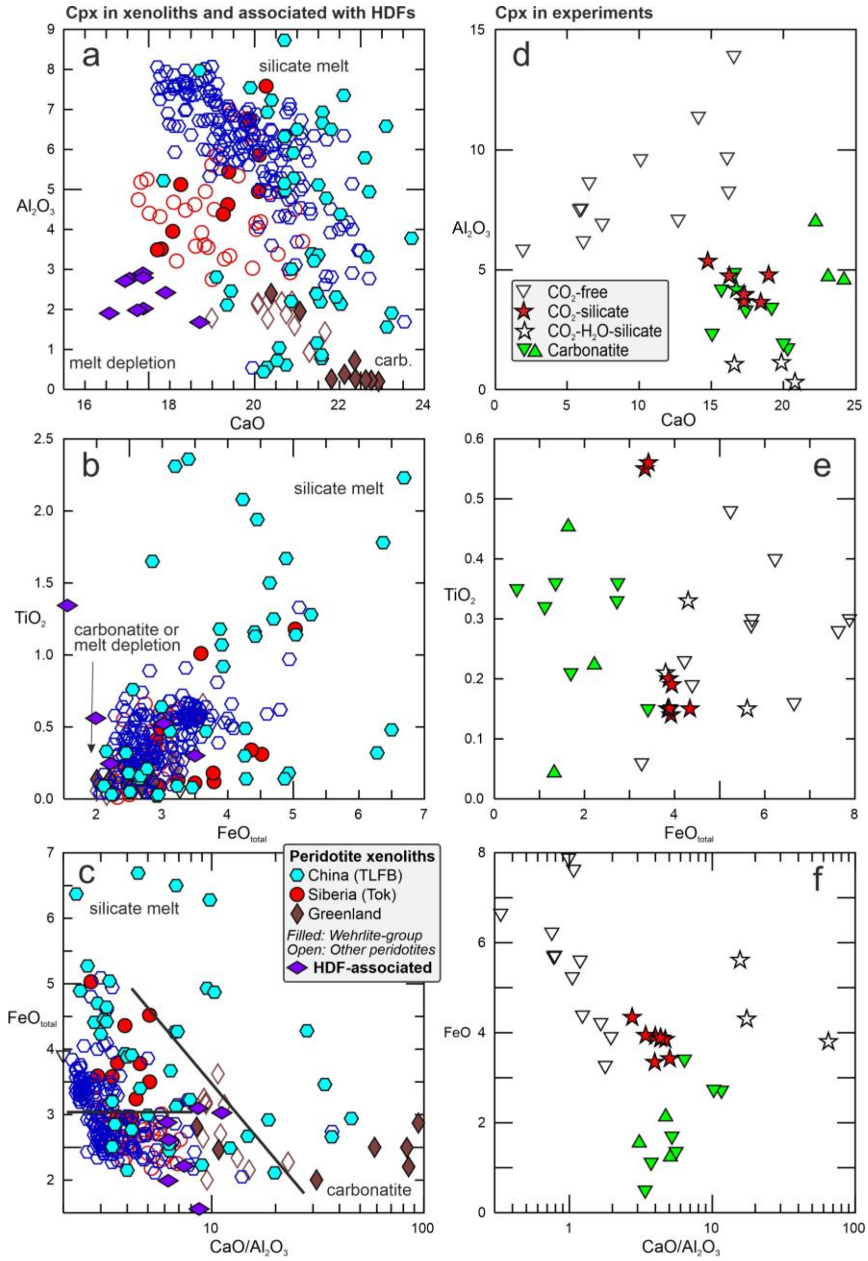

Figure S-2 Major-element relationships in clinopyroxene (cpx) from garnet-free xenolith suites (Table S-1) including wehrlite-group peridotites and other peridotites, as well as clinopyroxene occurring with diamond-hosted high-density fluids (HDF) **(a-c);** clinopyroxene or high-Ca pyroxene produced in experiments with variable amounts of $CO_2 \pm H_2O$ **(d-f)**. These relationships are used to illustrate varied effects of wehrlitisation depending on the nature of the metasomatic melt (silicate melt *vs.* carbonatite). For clarity, not all xenolith suites used in this study are shown. Depletion refers to melt extraction from peridotite. References: Tan Lu Fault Belt (TLFB): Xu *et al.* (1996, 1997, 1998), Zheng *et al.* (1998), Xu and Bodinier (2004), Hao *et al.* (2006, 2016), Yang *et al.* (2008), Liu *et al.* (2010), Xia *et al.* (2010), Xiao *et al.* (2010, 2013), Zhou *et al.* (2010), Lu *et al.* (2012), Wang *et al.* (2014), Lin *et al.* (2020); Aldan Shield in Siberia: Ionov *et al.* (2005a,b); North Atlantic craton in Greenland: Aulbach *et al.* (2017); clinopyroxene associated with HDF: Klein-BenDavid *et al.* (2009), Weiss *et al.* (2009, 2011, 2013, 2014), Weiss and Goldstein (2018). Experimental studies: Salters and Longhi (1999: open inverted triangles), Klemme *et al.* (1995: green triangles), Dasgupta *et al.* (2007: red stars, 2009: green inverted triangles), Girnis *et al*. (2013: open stars). Filled symbols denote wehrlite-group peridotites, open symbols denote lherzolites and harzburgites.

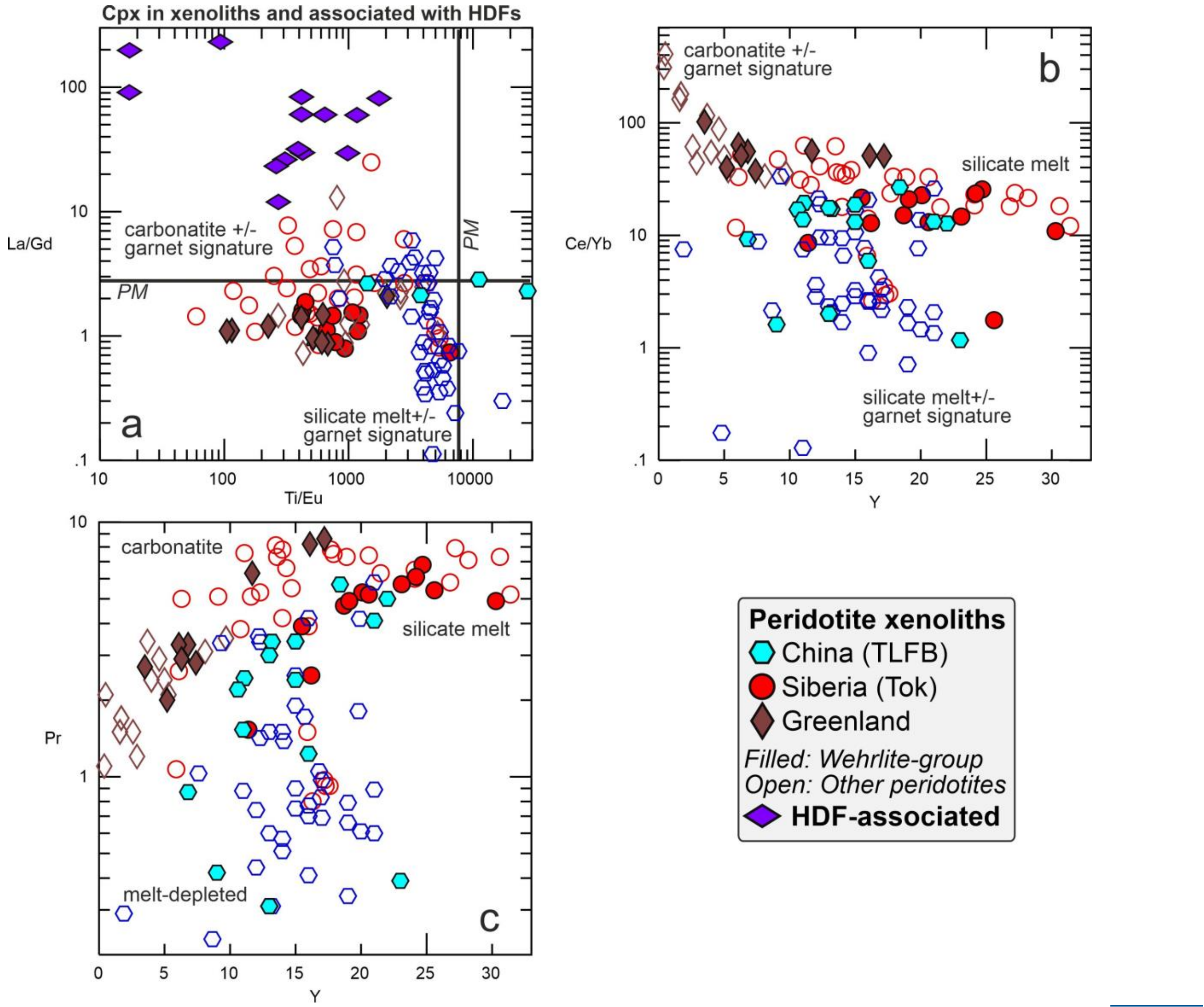

Figure S-3 **(a-c)** Trace-element relationships of clinopyroxene (cpx) in selected wehrlite-bearing peridotite xenolith suites reflecting processes and metasomatic agents as indicated in the panels, plus clinopyroxene associated with high-density fluids (HDFs) in diamond. References as in Figure S-2, Primitive Mantle PM of McDonough and Sun (1995).

Supplementary Information References

Abdelsalam, M.G., Gao, S.S., Liégeois, J.P. (2011) Upper mantle structure of the Saharan Metacraton. *Journal of African Earth Sciences* 60, 328-336.

Alasonati Tasárova, Z., Fullea, J., Bielik, M., Sroda, P. (2016) Lithospheric structure of Central Europe: Puzzle pieces of Pannonian Basin to Trans-European Suture Zone resolved by geophysical-petrological modelling. *Tectonics* 35, 733-753.

Artemieva, I.M. (2006) Global 1 degrees x 1 degrees thermal model TC1 for the continental lithosphere: Implications for lithosphere secular evolution. *Tectonophysics* 416, 245-277.

Artemieva, I.M. (2019) Lithosphere thermal thickness and geothermal heat flux in Greenland from a new thermal isostasy method. *Earth-Science Reviews* 188, 469–481.

Aulbach, S., Griffin, W.L., Pearson, N.J., O'Reilly, S.Y., Doyle, B.J. (2007) Lithosphere formation in the central Slave Craton (Canada): plume subcretion or lithosphere accretion? *Contributions to Mineralogy and Petrology* 154, 409-427.

Aulbach, S., Rudnick, R.L. (2009) Origins of non-equilibrium lithium isotopic fractionation in xenolithic peridotite minerals: Examples from Tanzania. *Chemical Geology* 258, 17-27.

Aulbach, S., Griffin, W.L., Pearson, N.J., O'Reilly, S.Y. (2013) Nature and timing of metasomatism in the stratified mantle lithosphere beneath the central Slave craton (Canada). *Chemical Geology* 352, 153-169.

Aulbach, S., Sun, J., Tappe, S., Höfer, H.E., Gerdes, A. (2017) Volatile-rich Metasomatism in the Cratonic Mantle beneath SW Greenland: Link to Kimberlites and Mid-lithospheric Discontinuities. *Journal of Petrology* 58, 2311-2338.

Beccaluva, L., Azzouni-Sekkal, A., Benhallou, A., Bianchini, G., Ellam, R.M., Marzola, M., Siena, F., Stuart, F.M. (2007) Intracratonic asthenosphere upwelling and lithosphere rejuvenation beneath the Hoggar swell (Alge- ria): Evidence from HIMU metasomatised lherzolite mantle xenoliths. *Earth and Planetary Science Letters* 260, 482-494.

Beccaluva, L., Bianchini, G., Ellam, R.M., Marzola, M., Oun, K.M., Siena, F., Stuart, F.M. (2008) The role of HIMU metasomatic components in the African lithospheric mantle: Petrological evidence from the Gharyan peridotite xenoliths, NW Libya. In: Coltorti, M. and Gregoire, M. Eds.), *etasomatism in Oceanic and Continental Lithospheric Mantle*. Geological Society of London Special Publication, London, 253-277.

Berkesi, M., Guzmics, T., Szabo´, C., Dubessy, J., Bodnar, R.J., Hidas, K., Ratter, K. (2012) The role of CO_2-rich fluids in trace element transport and metasomatism in the litho- spheric mantle beneath the Central Pannonian Basin, Hungary, based on fluid inclusions in mantle xenoliths. *Earth and Planetary Science Letters* 331, 8-20.

Boyd, F.R. (1974) Olivine megacrysts from the kimberlites of Monastery and Frank Smith Mines, South Africa. *Carnegie Institution of Washington Yearbook* 73, 282-285.

Boyd, F.R., Pokhilenko, N.P., Pearson, D.G., Mertzman, S.A., Sobolev, N.V., Finger, L.W. (1997) Composition of the Siberian cratonic mantle: evidence from Udachnaya peridotite xenoliths. *Contributions to Mineralogy and Petrology* 128, 228-246.

Cartwright, I., Weaver, T., Tweed, S., Ahearne, D., Cooper, M., Czapnik, K., Tranter, J. (2002) Stable isotope geochemistry of cold CO2-bearing mineral spring waters, Daylesford, Victoria, Australia: sources of gas and water and links with waning volcanism. *Chemical Geology* 185, 71-91.

Chanouan, L., Ikenne, M., Gahlan, H.A., Arai, S., Youbi, N. (2017) Petrological characteristics of mantle xenoliths from the Azrou- Timahdite quaternary basalts, middle atlas, Morocco: A mineral chemistry perspective. *Journal of African Earth Sciences* 127, 235-252.

Chen, L., Jiang, M.M., Yang, J.H., Wei, Z.G., Liu, C.Z., Ling, Y. (2014) Presence of an intralithospheric discontinuity in the central and western North China Craton: Implications for destruction of the craton. *Geology* 42, 223-226.

Chorowicz, J. (2005) The east African rift system. *Journal of African Earth Sciences* 43, 379-410.

Coltorti, M., Bonadiman, C., Hinton, R.W., Siena, F., Upton, B.G.J. (1999) Carbonatite metasomatism of the oceanic upper mantle: Evidence from clinopyroxenes and glasses in ultramafic xenoliths of Grande Comore, Indian Ocean. *Journal of Petrology* 40, 133-165.

Creighton, S., Stachel, T., Eichenberg, D., Luth, R.W. (2010) Oxidation state of the lithospheric mantle beneath Diavik diamond mine, central Slave craton, NWT, Canada. *Contributions to Mineralogy and Petrology* 159, 645-657.

Creighton, S., Stachel, T., McLean, H., Muehlenbachs, K., Simonetti, A., Eichenberg, D., Luth, R. (2008) Diamondiferous peridotitic microxenoliths from the Diavik Diamond Mine, NT. *Contributions to Mineralogy and Petrology* 155, 541-554.

Créon, L., Rouchon, V., Youssef, S., Rosenberg, E., Delpech, G., Szabó, C., Remusat, L., Mostefaoui, S., Asimow, P.D., Antoshechkina, P.M., Ghiorso, M.S., Boller, E., Guyot, F. (2017) Highly CO_2- supersaturated melts in the Pannonian lithospheric mantle – A transient carbon reservoir? *Lithos* 286-287, 519-533.

Dalton, J.A., Presnall, D.C. (1998) The continuum of primary carbonatitic-kimberlitic melt compositions in equilibrium with lherzolite: Data from the system CaO-MgO-Al_2O_3-SiO_2-CO_2 at 6 GPa. *Journal of Petrology* 39, 1953-1964.

Dautria, J.-M., Dupuy, C., Takherist, D., Dostal, J. (1992) Carbonate metasomatism in the lithospheric mantle: Peridotitic xenoliths from a melilititic district of the Sahara basin. *Contributions to Mineralogy and Petrology* 111, 37-52.

Danchin, R.V., Boyd, F.R. (1976) Ultramafic nodules from the Premier kimberlite pipe, South Africa. *Carnegie Institution of Washington Yearbook* 75, 531-538.

Dasgupta, R., Hirschmann, M.M., McDonough, W.F., Spiegelman, M., Withers, A.C. (2009) Trace element partitioning between garnet lherzolite and carbonatite at 6.6 and 8.6 GPa with applications to the geochemistry of the mantle and of mantle-derived melts. *Chemical Geology* 262, 57-77.

Davies, G.R., Lloyd, F.E. (1989) Pb-Sr-Nd isotope and trace element data bearing on the origin of the potassic subcontinental lithosphere beneath south-west Uganda, *Kimberlites and related rocks*. Geological Society of Australia Special Publication Blackwell, 784-794.

Dawson, J.B. (1984) Contrasting types of upper mantle metasomatism. In: Kornprobst, J. (Ed.), *Kimberlites. II. The mantle and crust-mantle relationships*. Elsevier, Amsterdam, 289-294.

Dèzes, P., Schmid, S.M., Ziegler, P.A. (2004) Evolution of the European Cenozoic Rift System; interaction of the Pyrenean and Alpine orogens with the foreland lithosphere. *Tectonophysics* 389, 1-33.

Downes, H., Macdonald, R., Upton, B.G.J., Cox, K.G., Bodinier, J.-L., Mason, P.R.D., James, D., Hill, P.G., Hearn, B.C.J. (2004) Ultramafic xenoliths from the Bearpaw Mountains, Montana, USA: evidence for mul- tiple metasomatic events in the lithospheric mantle beneath the Wyoming Craton. *Journal of Petrology* 45, 1631-1682.

Ehrenberg, S.N. (1982) Petrogenesis of Garnet Lherzolite and Megacrystalline Nodules from Thumb, Navajo Volcanic Field. *Journal of Petrology* 23, 507-547.

Faccini, B., Rizzo, A.L., Bonadiman, C., Ntaflos, T., Seghedi, I., Gregoire, M., Ferretti, G., Coltorti, M. (2020) Subduction-related melt refertilisation and alkaline metasomatism in the Eastern Transylvanian Basin lithospheric mantle: Evidence from mineral chemistry and noble gases in fluid inclusions,. *Lithos* 364-365, 105516.

Foley, S.F., Yaxley, G.M., Rosenthal, A., Buhre, S., Kiseeva, E.S., Rapp, R.P., Jacob, D.E. (2009) The composition of near-solidus melts of peridotite in the presence of CO2 and H2O between 40 and 60 kbar. *Lithos* 112, 274-283.

Franz, L., Brey, G.P., Okrusch, M. (1996) Reequilibration of ultramafic xenoliths from Namibia by metasomatic processes at the mantle boundary. *Journal of Geology* 104, 599-615.

Furman, T., Nelson, W.R., Elkins-Tanton, L.T. (2016) Evolution of the East African rift: Drip magmatism, lithospheric thinning and mafic volcanism. *Geochimica Et Cosmochimica Acta* 185, 418-434.

Geng, X.L., Foley, S.F., Liu, Y.S., Wang, Z.C., Hu, Z.C., Zhou, L. (2019) Thermal-chemical conditions of the North China Mesozoic lithospheric mantle and implication for the lithospheric thinning of cratons. *Earth and Planetary Science Letters* 516, 1-11.

Girnis, A.V., Bulatov, V.K., Brey, G.P. (2011) Formation of primary kimberlite melts - Constraints from experiments at 6-12 GPa and variable CO2/H2O. *Lithos* 127, 401-413.

Girnis, A.V., Bulatov, V.K., Brey, G.P., Gerdes, A., Hoefer, H.E. (2013) Trace element partitioning between mantle minerals and silico-carbonate melts at 6-12 GPa and applications to mantle metasomatism and kimberlite genesis. *Lithos* 160, 183-200.

Green, D.H., Wallace, M.E. (1988) Mantle metasomatism by ephemeral carbonatite melts. *Nature* 336, 459-462.

Grégoire, M., Tinguely, C., Bell, D.R., le Roex, A.P. (2005) Spinel lherzolite xenoliths from the Premier kimberlite (Kaapvaal craton, South Africa): Nature and evolution of the shallow upper mantle beneath the Bushveld complex. *Lithos* 84, 185-205.

Grütter, H.S., Gurney, J.J., Menzies, A.H., Winter, F. (2004) An updated classification scheme for mantle-derived garnet, for use by diamond explorers. *Lithos* 77, 841-857.

Hao, Y.T., Xia, Q.K., Yang, X.Z., Wang, R.C. (2006) Water in minerals of peridotite xenoliths from Cenozoic basalts in Nushan volcano, SE China (in Chinese with English abstract). *Acta Petrologica Sinica* 22, 1713-1722.

Hao, Y.T., Xia, Q.K., Jia, Z.B., Zhao, Q.C., Li, P., Feng, M., Liu, S.C. (2016) Regional heterogeneity in the water content of the Cenozoic lithospheric mantle of Eastern China. *Journal of Geophysical Research: Solid Earth* 121, 517-537.

Hearn, B.C. (2004) The Homestead kimberlite, central Montana, USA: mineralogy, xenocrysts, and upper-mantle xenoliths. *Lithos* 77, 473-491.

Hervig, R.L., Smith, J.V., Dawson, J.B. (1986) Lherzolite xenoliths in kimberlites and basalts: petrogenetic and crystallochemical significance of some minor and trace elements in olivine, pyroxenes, garnet and spinel. *Earth and Environmental Science Transactions of The Royal Society of Edinburgh* 77, 181-201.

Hin, R.C., Morel, M.L.A., Nebel, O., Mason, P.R.D., van Westrenen, W., Davies, G.R. (2009) Formation and temporal evolution of the Kalahari sub-cratonic lithospheric mantle: Constraints from Venetia xenoliths, South Africa. *Lithos* 112, 1069-1082.

Ionov, D.A., Chanefo, I., Bodinier, J.L. (2005a) Origin of Fe-rich lherzolites and wehrlites from Tok, SE Siberia by reactive melt percolation in refractory mantle peridotites. *Contributions to Mineralogy and Petrology* 150, 335-353.

Ionov, D.A., Chazot, G., Chauvel, C., Merlet, C., Bodinier, J.L. (2006) Trace element distribution in peridotite xenoliths from Tok, SE Siberian craton: A record of pervasive, multi-stage metasomatism in shallow refractory mantle. *Geochimica Et Cosmochimica Acta* 70, 1231-1260.

Ionov, D.A., Prikhodko, V.S., Bodinier, J.L., Sobolev, A.V., Weis, D. (2005b) Lithospheric mantle beneath the south-eastern Siberian craton: petrology of peridotite xenoliths in basalts from the Tokinsky Stanovik. *Contributions to Mineralogy and Petrology* 149, 647-665.

Ionov, D.A., Doucet, L.S., Ashchepkov, I.V. (2010) Composition of the Lithospheric Mantle in the Siberian Craton: New Constraints from Fresh Peridotites in the Udachnaya-East Kimberlite. *Journal of Petrology* 51, 2177-2210.

Ivanic, T.J., Harte, B., Gurney, J.J. (2012) Metamorphic re-equilibration and metasomatism of highly chromian, garnet-rich peridotitic xenoliths from South African kimberlites. *Contributions to Mineralogy and Petrology* 164, 505-520.

Ivanov, A.V., Vladykin, N.V., Demonterova, E.I., Gorovoy, V.A., Dokuchits, E.Y. (2018) $^{40}Ar/^{39}Ar$ Geochronology of the Malyy (Little) Murun Massif, Aldan Shield of the Siberian Craton: A Simple Story for an Intricate Igneous Complex. *Minerals* 8, 602.

Jolivet, M., De Boisgrollier, T., Petit, C., Fournier, M., Sankov, V.A., Ringenbach, J.-C., Byzov, L., Miroshnichenko, A.I., Kovalenko, S.N., Anisimova, S.V. (2009) How old is the Baikal Rift Zone? Insight from apatite fission track thermochronology. *Tectonics* 28, TC3008.

Jones, A.P., Smith, J.V., Dawson, J.B. (1983) Glasses in mantle xenoliths from Olmani, Tanzania. *Journal of Geology* 91, 167-178.

Kaczmarek, M.A., Bodinier, J.L., Bosch, D., Tommasi, A., Dautria, J.M., Kechid, S.A. (2016) Metasomatized Mantle Xenoliths as a Record of the Lithospheric Mantle Evolution of the Northern Edge of the Ahaggar Swell, In Teria (Algeria). *Journal of Petrology* 57, 345-382.

Karolyte, R., Johnson, G., Györe, D., Serno, S., Flude, S., Stuart, F.M., Chivas, A.R., Boyce, A., Gilfillan, S.M.V. (2019) Tracing the migration of mantle CO2 in gas fields and mineral water springs in south-east Australia using noble gas and stable isotopes. *Geochimica Et Cosmochimica Acta* 259, 109–128.

Klein-BenDavid, O., Izraeli, E.S., Hauri, E., Navon, O. (2007) Fluid inclusions in diamonds from the Diavik mine, Canada and the evolution of diamond-forming fluids. *Geochimica Et Cosmochimica Acta* 71, 723-744.

Klein-BenDavid, O., Logvinova, A.M., Schrauder, M., Spetsius, Z.V., Weiss, Y., Hauri, E.H., Kaminsky, F.V., Sobolev, N.V., Navon, O. (2009) High-Mg carbonatitic microinclusions in some Yakutian diamonds—a new type of diamond-forming fluid. *Lithos* 112, 648-659.

Klemme, S., Vanderlaan, S.R., Foley, S.F., Gunther, D. (1995) Experimentally-determined trace and minor element partitioning between clinpyroxene and carbonatite melt under upper-mantle conditions. *Earth and Planetary Science Letters* 133, 439-448.

Kopylova, M.G., Caro, G. (2004) Mantle xenoliths from the Southeastern Slave craton: Evidence for chemical zonation in a thick, cold lithosphere. *Journal of Petrology* 45, 1045-1067.

Kopylova, M.G., Russell, J.K., Cookenboo, H. (1999) Petrology of peridotite and pyroxenite xenoliths from the Jericho kimberlite: Implications for the thermal state of the mantle beneath the Slave craton, Northern Canada. *Journal of Petrology* 40, 79-104.

Kourim, F., Bodinier, J.L., Alard, O., Bendaoud, A., Vauchez, A., Dautria, J.M. (2014) Nature and evolution of the litho- spheric mantle beneath the Hoggar Swell (Algeria): a record from mantle xenoliths. *Journal of Petrology* 55, 2249-2280.

Kumar, P., Kind, R., Hanka, W., Wylegalla, K., Reigber, C., Yuan, X., Woelbern, I., Schwintzer, P., Fleming, K., Dahl-Jensen, T., Larsen, T.B., Schweitzer, J., Priestley, K., Gudmundsson, O., Wolf, D. (2005) The lithosphere-asthenosphere boundary in the North-West Atlantic region. *Earth and Planetary Science Letters* 236, 249-257.

Lee, C.-T., Rudnick, R.L. (1999) Compositionally stratified cratonic lithosphere: Petrology and geochemistry of peridotite xenoliths from the Labait Voclcano, Tanzania, *Proceedings of the 7th International Kimberlite Conference*. Red Roof Design cc, Cape Town, 503-521.

Lee, C.T.A. (2003) Compositional variation of density and seismic velocities in natural peridotites at STP conditions: Implications for seismic imaging of compositional heterogeneities in the upper mantle. *Journal of Geophysical Research-Solid Earth* 108, 2441.

Liégeois, J.P., Benhallou, A., Azzouni-Sekkal, A., Yahiaoui, R., Bonin, B. (2005) The Hoggar swell and volcanism: reactivation of the Precambrian Tuareg shield during Alpine convergence and West African Cenozoic volcanism. In: Foulger, G.R., Natland, J.H., Presnall, D.C., and Anderson, D.L. Eds.), *Plates Plumes and Paradigms*. Geological Society of America Special Paper, 379-400.

Liégeois, J.P., Latouche, L., Boughrara, M., Navez, J., Guiraud, M. (2003) The LATEA metacraton (Central Hoggar, Tuareg shield, Algeria): behaviour of an old passive margin during the Pan-African orogeny. *Journal of African Earth Sciences* 37, 161-190.

Liptai, N., Patkó, L., Kovács, I.J., Hidas, K., Pintér, Z., Jeffries, T., Zajacz, Z., O'Reilly, S.Y., Griffin, W.L., Pearson, N.J., Szabó, C. (2017) Multiple metasomatism beneath the Nógrád–Gömör Volcanic Field (Northern Pannonian Basin) revealed by upper mantle peridotite xenoliths. *Journal of Petrology* 58, 1107-1144.

Liu, Z.C., Wu, F.Y., Chu, Z.Y., Xu, X.S. (2010) Isotopic compositions of the peridotitic xenoliths from the Nushan, Anhui Province: Constraints on the age of subcontinental lithospheric mantle beneath the East China (in Chinese with English abstract). *Acta Petrologica Sinica* 26, 1217-1240.

Lu, S.M., Pei, F.P., Zhou, Q.J., Jin, K., Peng, Y.J., Chen, Y., Xu, W.L. (2012) Origin of late Mesozoic alkaline basalts and nature of lithospheric mantle in Liaoyuan area, Jilin province (in Chinese with English abstract). *Earth Science–Journal of China University of Geosciences* 37, 475-488.

MacKenzie, J.M., Canil, D. (1999) Composition and thermal evolution of cratonic mantle beneath the central Archean Slave Province, NWT, Canada. *Contributions to Mineralogy and Petrology* 134, 313-324.

McDonough, W.F., Sun, S.-s. (1995) The composition of the Earth: Chemical Evolution of the Mantle. *Chemical Geology* 120, 223-253.

Menzies, A., Westerlund, K., Grütter, H., Gurney, J., Carlson, J., Fung, A., Nowicki, T. (2004) Peridotitic mantle xenoliths from kimberlites on the Ekati Diamond Mine property, NWT, Canada: major element compositions and implications for the lithosphere beneath the central Slave craton. *Lithos* 77, 395-412.

Mitchell, R.H. (1984) Garnet lherzolites from Hanaus-I and Louwrensia kimberlites of Namibia. *Contributions to Mineralogy and Petrology* 86, 178-188.

Nielsen, L.J., Hutchison, M.T., Malarkey, J. (2008) Geothermal constraints from kimberlite-hosted garnet lherzolites from southern Greenland. *9th International Kimberlite Conference* (Frankfurt, Germany),

Ntaflos, T., Bizimis, M., Abart, R. (2017) Mantle xenoliths from Szentbékálla, Balaton: Geochemical and petrological constraints on the evolution of the lithospheric mantle underneath Pannonian Basin, Hungary. *Lithos* 276, 30-44.

Oostingh, K.F., Jourdan, F., Merle, R., Chiaradia, M. (2016) Spatio-temporal Geochemical Evolution of the SE Australian Upper Mantle Deciphered from the Sr, Nd and Pb Isotope Compositions of Cenozoic Intraplate Volcanic Rocks. *Journal of Petrology* 57, 1509–1530.

Patko, L., Aradi, L.E., Liptai, N., Bodnar, R.J., Fedele, L., Kovacs, Z., Cesare, B., Vaselli, O., Fioretti, A.M., Jeffries, T., Szabo, C. (2013) Wehrlitization processes within the upper mantle beneath the Northern Pannonian Basin (Hungary). *Mineralogical Magazine* 77, 1934.

Patkó, L., Liptai, N., Kovács, I.J., Aradi, L., Xia, Q.-K., Ingrin, J., Mihály, J., O'Reilly, S., Griffin, W.L., Wesztergom, V., Szabó, C. (2019) Extremely low structural hydroxyl contents in upper mantle xenoliths from the Nógrád-Gömör Volcanic Field (northern Pannonian Basin): geodynamic implications and the role of post-eruptive re-equilibration. *Chemical Geology* 1302, 23–41.

Patkó, L., Liptai, N., Kovács, I.J., Aradi, L.E., Xia, Q.-K., Ingrin, J., Mihály, J., O'Reilly, S.Y., Griffin, W.L., Wesztergom, V., Szabó, C. (2020) Extremely low structural hydroxyl contents in upper mantle xenoliths from the Nógrád-Gömör Volcanic Field (northern Pannonian Basin): Geodynamic implications and the role of post-eruptive re-equilibration. *Chemical Geology* 507, 23–41.

Priestley, K., Debayle, E. (2003) Seismic evidence for a moderately thick lithosphere beneath the Siberian Platform. *Geophysical Research Letters* 30, 1118.

Raffone, N., Chazot, G., Pin, C., Vannucci, R., Zanetti, A. (2009) Metasomatism in the lithospheric mantle beneath Middle Atlas (Morocco) and the origin of Fe- and Mg-rich wehrlites. *Journal of Petrology* 50, 197-249.

Rehfeldt, T., Foley, S.F., Jacob, D.E., Carlson, R.W., Lowry, D. (2008) Contrasting types of metasomatism in dunite, wehrlite and websterite xenoliths from Kimberley, South Africa. *Geochimica Et Cosmochimica Acta* 72, 5722-5756.

Rudnick, R.L., Donough, W.L., Orpin, A. (1994) Northern Tanzanian peridotite xenoliths: a comparison with Kaapvaal peridotites and inferences on metasomatic interactions. In: Meyer, H.O.A. (Ed.) *Kimberlites, related rocks and mantle xenoliths*. CPRM Special Publication, Brasilia, 336-353.

Rudnick, R.L., McDonough, W.F., Chappell, B.W. (1993) Carbonatite metasomatism in the northern Tanzanian mantle - petrographic and geochemical characteristics. *Earth and Planetary Science Letters* 114, 463-475.

Salters, V.J.M., Longhi, J. (1999) Trace element partitioning during the initial stages of melting beneath mid-ocean ridges. *Earth and Planetary Science Letters* 166, 15-30.

Schmidberger, S.S., Francis, D. (2001) Constraints on the trace element composition of the Archean mantle root beneath Somerset Island, Arctic Canada. *Journal of Petrology* 42, 1095-1117.

Simon, N.S.C., Carlson, R.W., Pearson, D.G., Davies, G.R. (2007) The origin and evolution of the Kaapvaal cratonic lithospheric mantle. *Journal of Petrology* 48, 589-625.

Sobolev, N.V., Pokhilenko, N.P., Yefimova, E.S. (1984) Xenoliths of diamond-bearing peridotites in kimberlites, the problem of diamond origin. *Geology and Geophysics (in Russian)* 12, 63-80.

Stachel, T., Harris, J.W. (2008) The origin of cratonic diamonds - Constraints from mineral inclusions. *Ore Geology Reviews* 34, 5-32.

Stachel, T., Viljoen, K.S., Brey, G., Harris, J.W. (1998) Metasomatic processes in lherzolitic and harzburgitic domains of diamondiferous lithospheric mantle: REE in garnets from xenoliths and inclusions in diamonds. *Earth and Planetary Science Letters* 159, 1-12.

Stagno, V., Ojwang, D.O., McCammon, C.A., Frost, D.J. (2013) The oxidation state of the mantle and the extraction of carbon from Earth's interior. *Nature* 493, 84-88.

Stamm, N., Schmidt, M.W. (2017) Asthenospheric kimberlites: Volatile contents and bulk compositions at 7 GPa. *Earth and Planetary Science Letters* 474, 309-321.

Streckeisen, A. (1976) To each plutonic rock its proper name. *Earth-Science Reviews* 12, 1-33.

Suhr, G., Hellebrand, E., Snow, J.E., Seck, H.A., Hofmann, A.W. (2003) Significance of large, refractory dunite bodies in the upper mantle of the Bay of Islands Ophiolite. *Geochemistry Geophysics Geosystems* 4, 8605.

Szabo, C., Falus, G., Zajacz, Z., Kovacs, I., Bali, E. (2004) Composition and evolution of lithosphere beneath the Carpathian-Pannonian Region: a review. *Tectonophysics* 393, 119-137.

Tappe, S., Steenfelt, A., Nielsen, T. (2012) Asthenospheric source of Neoproterozoic and Mesozoic kimberlites from the North Atlantic craton, West Greenland: New high-precision U-Pb and Sr-Nd isotope data on perovskite. *Chemical Geology* 320, 113-127.

Tiberi, C., Diament, M., Deverchere, J., Petit-Mariani, C., Mikhailov, V., Tikhotsky, S., Achauer, U. (2003) Deep structure of the Baikal rift zone revealed by joint inversion of gravity and seismology. *Journal of Geophysical Research* 108, 2133.

Timmerman, S., Honda, M., Phillips, D., Jaques, A.L., Harris, J.W. (2018) Noble gas geochemistry of fluid inclusions in South African diamonds: implications for the origin of diamond-forming fluids. *Mineralogy and Petrology* 112, 181-195.

Trieloff, M., Altherr, R. (2007) He-Ne-Ar Isotope Systematics of Eifel and Pannonian Basin Mantle Xenoliths Trace Deep Mantle Plume-Lithosphere Interaction Beneath the European Continent. In: Ritter, J.R.R., Christensen, U.R. (Eds.) *Mantle Plumes*. Springer, Berlin, Heidelberg, 339-367,

Viljoen, K.S., Robinson, D.N., Swash, P.M., Griffin, W.L., Otter, M.L., Ryan, C.G., Win, T.T. (1994) Diamond- and graphite-bearing peridotite xenoliths from the Roberts Victor kimber- lite, South Africa. In: Meyer, H.O.A. and Leonardos, O.H. Eds.), *Kimberlites, Related Rocks and Mantle Xenoliths. Proceedings of the Fifth International Kimberlite Conference*. Companhia de Pesquisa de Recursos Minerais Special Publication, Brasilia, 285-303.

Walter, M.J. (2014) Melt extraction and compositional variability in mantle lithosphere. In: Holland, H.D., Turekian, K.K., and Carlson, R.W. Eds.), *Treatise on Geochemistry (2nd edition). Volume 3: The Mantle and the Core*. Elsevier Pergamon, Amsterdam, 393-419.

Wang, Q., Bagdassarov, N., Xia, Q.K., Zhu, B. (2014) Water contents and electrical conductivity of peridotite xenoliths from the North China Craton: Implications for water distribution in the upper mantle. *Lithos* 189, 105-126.

Weeraratne, D.S., Forsyth, D.W., Fischer, K.M., Nyblade, A.A. (2003) Evidence for an upper mantle plume beneath the Tanzanian craton from Rayleigh wave tomography. *Journal of Geophysical Research-Solid Earth* 108, 2427.

Weiss, Y., Goldstein, S.L. (2018) The involvement of diamond-forming fluids in the metasomatic "cocktail' of kimberlite sources. *Mineralogy and Petrology* 112, 149-167.

Weiss, Y., Kessel, R., Griffin, W.L., Kiflawi, I., Klein-BenDavid, O., Bell, D.R., Harris, J.W., Navon, O. (2009) A new model for the evolution of diamond-forming fluids: Evidence from microinclusion-bearing diamonds from Kankan, Guinea. *Lithos* 112, 660-674.

Weiss, Y., Griffin, W.L., Bell, D.R., Navon, O. (2011) High-Mg carbonatitic melts in diamonds, kimberlites and the sub-continental lithosphere. *Earth and Planetary Science Letters* 309, 337-347.

Weiss, Y., Griffin, W.L., Navon, O. (2013) Diamond-forming fluids in fibrous diamonds: The trace-element perspective. *Earth and Planetary Science Letters* 376, 110-125.

Weiss, Y., Kiflawi, I., Davies, N., Navon, O. (2014) High-density fluids and the growth of monocrystalline diamonds. *Geochimica Et Cosmochimica Acta* 141, 145-159.

Westerlund, K.J., Shirey, S.B., Richardson, S.H., Carlson, R.W., Gurney, J.J., Harris, J.W. (2006) A subduction wedge origin for Paleoarchean peridotitic diamonds and harzburgites from the Panda kimberlite, Slave craton: evidence from Re-Os isotope systematics. *Contributions to Mineralogy and Petrology* 152, 275-294.

Winterburn, P.A., Harte, B., Gurney, J.J. (1990) Peridotite xenoliths from the Jagersfontein kimberlite pipe: I. Primary and primary–metasomatic mineralogy. *Geochimica Et Cosmochimica Acta* 54, 329-341.

Witt-Eickschen, G., O'Neill, H.S. (2005) The effect of temperature on the equilibrium distribution of trace elements between clinopyroxene, orthopyroxene, olivine and spinel in upper mantle peridotite. *Chemical Geology* 221, 65-101.

Witt-Eickschen, G., Kaminsky, W., Kramm, U., Harte, B. (1998) The nature of young vein metasomatism in the lithosphere of the West Eifel (Germany): Geochemical and isotopic constraints from composite mantle xenoliths from the Meerfelder Maar. *Journal of Petrology* 39, 155-185.

Witt-Eickschen, G., Seck, H.A., Mezger, K., Eggins, S.M., Altherr, R. (2003) Lithospheric mantle evolution beneath the Eifel (Germany): Constraints from Sr-Nd-Pb isotopes and trace element abundances in spinel peridotite and pyroxenite xenoliths. *Journal of Petrology* 44, 1077-1095.

Wittig, N., Pearson, D.G., Baker, J.A., Duggen, S., Hoernle, K. (2010) A major element, PGE and Re-Os isotope study of Middle Atlas (Morocco) peridotite xenoliths: Evidence for coupled introduction of metasomatic sulphides and clinopyroxene. *Lithos* 115, 15-26.

Wölbern, I., Rumpker, G., Link, K., Sodoudi, F. (2012) Melt infiltration of the lower lithosphere beneath the Tanzania craton and the Albertine rift inferred from S receiver functions. *Geochemistry Geophysics Geosystems* 13, 8103.

Woodland, A.B., Koch, M. (2003) Variation in oxygen fugacity with depth in the upper mantle beneath the Kaapvaal craton, Southern Africa. *Earth and Planetary Science Letters* 214, 295-310.

Xia, Q.K., Hao, Y.T., Li, P., Deloule, E., Coltorti, M., Dallai, L., Yang, X.Z., Feng, M. (2010) Low water content of the Cenozoic lithospheric mantle beneath the eastern part of the North China Craton. *Journal of Geophysical Research: Solid Earth* 115(B7), B07207.

Xiao, Y., Teng, F.Z., Zhang, H.F., Yang, W. (2013) Large magnesium isotope fractionation in peridotite xenoliths from eastern North China craton: Product of melt–rock interaction. *Geochimica Et Cosmochimica Acta* 115, 241-261.

Xiao, Y., Zhang, H.F., Fan, W.M., Ying, J.F., Zhang, J., Zhao, X.M., Su, B.X. (2010) Evolution of lithospheric mantle beneath the Tan-Lu fault zone, eastern North China Craton: evidence from petrology and geochemistry of peridotite xenoliths. *Lithos* 117, 229-246.

Xu, J., Zhu, G., Tong, W., Kerei, C., Liu, Q. (1987) Formation and evolution of the Tancheng-Lujiang wrench fault system: a major shear system to the northwest of the Pacific Ocean. *Tectonophysics* 134, 273-310.

Xu, X.S., O'Reilly, S.Y., Griffin, W.L., Zhou, X.M., Huang, X.L. (1998) The Nature of the Cenozoic Lithosphere at Nushan, Eastern China. In: Flower, M.F.J., Chung, S.J., Lo, C.H., Lee, T.Y. (Eds.) *Mantle Dynamics and Plate Interactions in East Asia*. American Geophysical Union, Geodynamics Series, 167-195.

Xu, Y.G., Bodinier, J.L. (2004) Contrasting enrichments in high-and low-temperature mantle xenoliths from Nushan, Eastern China: results of a single metasomatic event during lithospheric accretion? *Journal of Petrology* 45, 321-341.

Xu, Y.G., Mercier, J.C., Lin, C.Y. (1997) Amphibole-bearing peridotite xenoliths from Nushan, Anhui Province: evidence for melt percolation process in the upper mantle and lithospheric uplift. *Chinese Journal of Geochemistry* 16, 213-229.

Xu, Y.G., Mercier, J.C.C., Menzies, M.A., Ross, J.V., Harte, B., Lin, C.Y., Shi, L.B. (1996) K-rich glass-bearing wehrlite xenoliths from Yitong, northeastern China: petrological and chemical evidence for mantle metasomatism. *Contributions to Mineralogy and Petrology* 125, 406-420.

Yang, X.Z., Xia, Q.K., Deloule, E., Dallai, L., Fan, Q.C., Feng, M. (2008) Water in minerals of the continental lithospheric mantle and overlying lower crust: a comparative study of peridotite and granulite xenoliths from the North China Craton. *Chemical Geology* 258, 33-45.

Yaxley, G.M., Berry, A.J., Rosenthal, A., Woodland, A.B., Paterson, D. (2017) Redox preconditioning deep cratonic lithosphere for kimberlite genesis - evidence from the central Slave Craton. *Scientific Reports* 7, 30.

Yaxley, G.M., Crawford, A.J., Green, D.H. (1991) Evidence for carbonatite metasomatism in spinel peridotite xenoliths from western Victoria, Australia. *Earth and Planetary Science Letters* 107, 305-317.

Zhang, S.-B., Rudnick, R., McCammon, C. (2017) Oxidation of lithospheric mantle beneath Tanzania by melt reaction. *11th International Kimberlite Conference* (Gaborone, Botswana),

Zheng, J.P., O'Reilly, S.Y., Griffin, W.L., Lu, F.X., Zhang, M. (1998) Nature and evolution of Cenozoic lithospheric mantle beneath Shandong peninsula, Sino-Korean craton, eastern China. *International Geology Review* 40, 471-499.

Zhou, Q., Wu, F.Y., Chu, Z.Y., Ge, W.C. (2010) Isotopic compositions of mantle xenoliths and age of the lithospheric mantle in Yitong, Jilin Province (in Chinese with English abstract). *Acta Petrologica Sinica* 26, 1241–1264.

Zhu, G., Liu, C., Gu, C., Zhang, S., Li, Y., Su, N., Xiao, S. (2018) Oceanic plate subduction history in the western Pacific Ocean: Constraint from the Late Mesozoic evolution of the Tan-Lu Fault Zone. *Science China-Earth Sciences* 61, 386-405.

Ziegler, P.A., Dèzes, P. (2005) Evolution of the lithosphere in the area of the Rhine Rift System. *International Journal of Earth Sciences* 94, 594-614.

Zinngrebe, E., Foley, S.F. (1995) Metasomatism in mantle xenoliths from Gees, West Eifel, Germany: evidence of calc-alkaline glasses and metasomatic Ca-enrichment. *Contributions to Mineralogy and Petrology* 122, 79-96.